Fall 10-31-1995

Chute flow experiments

Yahong Zhang
New Jersey Institute of Technology

Copyright Warning & Restrictions

The copyright law of the United States (Title 17, United States Code) governs the making of photocopies or other reproductions of copyrighted material.

Under certain conditions specified in the law, libraries and archives are authorized to furnish a photocopy or other reproduction. One of these specified conditions is that the photocopy or reproduction is not to be "used for any purpose other than private study, scholarship, or research." If a, user makes a request for, or later uses, a photocopy or reproduction for purposes in excess of "fair use" that user may be liable for copyright infringement,

This institution reserves the right to refuse to accept a copying order if, in its judgment, fulfillment of the order would involve violation of copyright law.

Please Note: The author retains the copyright while the New Jersey Institute of Technology reserves the right to distribute this thesis or dissertation

Printing note: If you do not wish to print this page, then select "Pages from: first page # to: last page #" on the print dialog screen

ABSTRACT

CHUTE FLOW EXPERIMENTS

by
Yahong Zhang

The objective of this thesis is to study the behavior of granular materials flowing down an inclined chute using three diagnostic techniques under different chute inclination angles and chute floor conditions. The three methods are: (1) tracking the motion of single particle within the mass in a noninvasive manner using a transmitting sphere and antenna receiving system, (2) scale mass flow rate measurement, and (3) high speed camera system to obtain flow velocity measurements.

For these purposes, an experimental setup has been completed and a set experiments has been performed.

CHUTE FLOW EXPERIMENTS

by
Yahong Zhang

A Thesis
Submitted to the Faculty of
New Jersey Institute of Technology
in Partial Fulfillment of the Requirement for the Degree of
Master of Science in Mechanical Engineering

Department of Mechanical Engineering

October 1995

APPROVAL PAGE

CHUTE FLOW EXPERIMENTS

Yahong Zhang

Dr. Anthony D. Rosato, Thesis Advisor — Date
Associate Professor of Mechanical Engineering,
New Jersey Institute of Technology

Dr. Rong Y. Chen, Committee Member — Date
Professor of Mechanical Engineering,
New Jersey Institute of Technology

Dr. Rajesh N. Dave, Committee Member — Date
Associate Professor of Mechanical Engineering,
New Jersey Institute of Technology

Dr. Ian S. Fischer, Committee Member — Date
Associate Professor of Mechanical Engineering,
New Jersey Institute of Technology

BIOGRAPHICAL SKETCH

Author: Yahong Zhang

Degree: Master of Science in Mechanical Engineering

Date: October 1995

Undergraduate and Graduate Education:

- Master of Science in Mechanical Engineering,
  New Jersey Institute of Technology,
  Newark, New Jersey, 1995

- Bachelor of Science in Power Machinery Engineering
  Jiaotong University
  Shanghai, P. R. China, 1980

Major: Mechanical Engineering

Presentation and Publications:

Zhang, Yahong (1995).
Chute Flow Experiments.
Proceedings of the FIFTH ASME Region II Graduate Student Technical Conference.
Rutgers University, New Brunswick, New Jersey.

Zhang, Yahong (1991).
A Novel Approach to Air-conditioning.
Automobile & Tractor. Volume 4.

Zhang, Yahong (1988).
Some Heat Transfer Factors, Analysis and Calculations Which Should Be Considered in Automobile Air-conditioning Evaluation.
Automobile & Tractor. Volume 3.

This thesis is dedicated to my husband, my daughter, and my parents for their support and patience during my study abroad.

ACKNOWLEDGMENT

I would like to express my sincere gratitude to my advisor, Dr. Anthony D. Rosato for his direction and support throughout this research. I would also like to thank Drs. Rong Y. Chen, Rajesh N. Dave, and Ian S. Fischer for serving as committee members and helping me in this work.

I acknowledge Songyao Ren, Vivek Gupta, Anthony La Rosa, Don Rosander, Jack Gidney, Joe Glaz, Dave Singh, Anthony Troiano, Jerry Volcy, Yidan Lan, Heng Yung, Guanghua Chu, Jitesh Agrawal, Ezekiel Opeola, Laurent R. Labous, and Prashant Patel for their support during this research.

Finally, I am grateful to the United States Department of Energy for having funded this project and I am thankful for the financial support from the Mechanical Engineering Department and the Particulate Flow Laboratory of New Jersey Institute of Technology.

TABLE OF CONTENTS

TABLE OF CONTENTS
(Continued)

TABLE OF CONTENTS
(Continued)

LIST OF FIGURE

LIST OF FIGURES
(Continued)

Figure Page

LIST OF FIGURES
(Continued)

Figure **Page**

CHAPTER 1

INTRODUCTION

1.1 The Study of Granular Materials

The terms granular materials or bulk solids refer to mixtures made up of discrete solid particles which are dispersed in a fluid phase. Bulk solid comprise one member of a larger class of two-phase disperse systems made up of solids and fluids when dilute suspensions form another related member. The fluid phase has relatively less influence on bulk solids while it plays a major role in determining the dynamics of dilute suspensions which will not be discussed in this thesis. In situations involving the flow and yielding of such bulk materials, the typical solids concentrations are quite high and the solid constituents come in contact with their neighbors. Direct interactions between the individual solid constituents are frequent, the bulk behavior is governed largely by interparticle forces, friction, and collisions. In some instances the effects of the interactions between the fluid and solid components may be small because the interstitial fluid has relatively small density and viscosity, as in the case of a gas. In general, the material behavior is very complex, and its understanding requires the melding of ideas from traditional solid mechanics, fluid mechanics, elasticity theory, plasticity theory, soil mechanics, rheology, and kinetic gas theory[Savage(1984)].

Granular materials or bulk solids occur in various forms: dry grains and powders, slurries, suspensions or pastes. Some examples are sand, ore, mineral concentrate, coal,

crushed oil shale, grain animal feed, foodstuffs, pharmaceuticals, granular snow, pack ice, metal powder and ceramic powder. Although there are some instances and flow regimes in which the interstitial fluid can be important, the essential feature of them is the interaction between the solid particles.

A great deal is known about granular materials in a static state or undergoing slow deformations. However, the present understanding of granular materials which are flowing rapidly is much more rudimentary. Because of its formidable nature, the scientific development of the subject has lagged behind that associated with simpler and more conventional, single phase, continuum fluids. There are many unsolved problems, in some cases even a qualitative understanding of the flow phenomenon is lacking [Savage(1992)].

The research of the mechanics of the flow of these kinds of materials is essential for the understanding and solution of a wide range of technological and scientific problems related to materials-handling engineering, pneumatic transport, flows in slurry pipelines, mineral and powder processing, fluidized bed combustion of coal and wastes, stability of tailings dumps, flow in peddle bed nuclear reactions, rock falls, debris flows, subaqueous grain flows, snow avalanches, ice jams, drift of pack ice, sediment transport in rivers, dynamics of planetary rings, and sand transport under the feet of astronaut in the moon, etc.

Historically, the dynamics of flowing granular materials has been previously observed in inclined chutes by Savage, Johnson, Ahn, and Hanes[Hanes(1992)]. The chute flow experiments we are doing now have their new characteristics which will be described in the following content.

1.2 Statement of the Problem

The objective of this thesis is to study the behavior of granular materials flowing down an inclined chute using three diagnostic techniques under different chute inclination angles and chute flow conditions. The three methods are: (1) tracking the motion of single particle within the mass in a noninvasive manner using a transmitting sphere and antenna receiving system, (2) scale mass flow rate measurement, and (3) high speed camera system to obtain flow velocity measurements.

For these purposes, an experimental setup has been completed. It includes chute, hopper, hopper frame, exit box, scale, and vacuum conveyor, etc. An innovative and nonintrusive particle tracking system have been developed under the support of U. S. Department of Energy. The tracking experiments are based on the excellent results obtained in the free fall test. The theoretical viability of this tracking system has been substantiated by Dave[Dave(1992)].

Many experiments have been performed under different chute inclination angles and chute floor conditions for the comparison purpose. The chute inclination angles used in our experiments are 8.8 degrees, 10.8 degrees, 13.7 degrees, and 15 degrees. The chute floor has been changed in the form of either smooth or bumpy. Some of the experimental results are meaningful (see **CHAPTER 5**).

1.3 Outline of Remaining Chapters

In Chapter two, we discuss the mechanics principle of granular material flow in the scope as constitutive behavior, mechanisms for generation of stresses, flow regimes, kinetic

theories, flow mode and dimensional analysis, some important physical concepts, and some analysis for inclined chute flow. Chapter three describes experimental set-up with respect to hopper, entrance, chute, exit, scale system and other apparatus. In Chapter four, we focus on the particle tracking technique and its authentic application on the chute flow experiments. In Chapter five, we present experiment procedures and results. They are scale data acquisition and mass flow rate, high speed camera system and flow velocity, Distribution of flow layers, and tracking sphere experiment steps. Chapter six summarizes the progress and discusses the direction of future work. Besides, the conclusion is provided.

CHAPTER 2

MECHANICS PRINCIPLE OF GRANULAR MATERIAL FLOW

2.1 General Discussion of Constitutive Behavior

Our discussion from a brief description of some aspects of the constitutive behavior of granular materials. To perform analyses of various flow situations, we eventually require continuum descriptions of the constitutive equations for the fluxes of mass, momentum and energy. However, to obtain a better physical understanding of the bulk behavior, it is sometimes necessary to focus at a finer scale and consider things at the level of individual particle interactions. This approach can be pursued further to obtain analytical descriptions in terms of kinetic theories for this bulk behavior.

2.2 Mechanisms for Generation of Stresses

To simplify these preliminary remarks, we shall consider the bulk to be made up of solid particles immersed in a gas of negligible density so that we can ignore any interstitial fluid effects. During deformation of the bulk material, individual particles typically acquire, in addition to their mean translational motion, more or less random translational fluctuation velocity and spins, as a result of collisions and particle overriding. For dry granular materials, there are three main mechanisms by which stresses can be generated during bulk deformations; these are:

(1) dry Coulomb-type rubbing friction;

(2) transport of momentum by particle translation;

(3) momentum transport by collisional interactions.

Similar mechanisms are at work during the analogous transport of energy, etc.

Although there are instances where all three of these mechanisms are effective, there limiting regimes in which a single one plays the dominant role which we shall discuss in 2.3.1. At high solids concentrations and low shear rates, the particles will be in close rubbing contact and the stresses are of the quasi-static, rate-independent Coulomb-type described in the soil mechanics literature. On the other hand at very low concentrations and high shear rates. The granular material will be in some ways analogous to a dilute gas. The mean free path is large compared to the particle diameter, and stresses result from the interchange of particles between adjacent layers moving at different mean transport velocities. If both the concentration and shear rate are large, then momentum transport occurs as a result of collisional interactions, since there rarely occur void spaces of sufficient size to permit particle transport between adjacent shear layers.

2.3 Mechanics Theories

2.3.1 Granular Flow Regimes

Granular flows can be classified in terms of different flow regimes, each having distinct characteristics. The main emphasis of this review is on the rapid flow regime, in which the effects of particle grain inertia are dominant. But for some reasons, sometimes, one kinds flow behavior exists in other flow regimes. For example, in some cases of granular flow, portions of the granular material may be "locked" together and nearly rigid, the mechanics

of deformation of these portions is different from those where grain inertia is important. In some cases, interstitial fluid viscosity and density may be important.

To better the classification, Bagnold did his pioneering work on granular flow and gave his definition in 1954[Savage(1984)]. From his experiment, he was able to define the various flow regimes in term N (Which is named "Bagnold Number" lately.). That is:

$$N = \lambda^{1/2} \rho_f d^2 (u_{1,2}) / \mu \qquad (2\text{-}1)$$

where ρ_f : mass density

μ : viscosity

d : particle diameter

$u_{1,2}$: velocity gradient

λ : linear concentration of particles

N<40 corresponded to the macroviscous regime; N>450 corresponded to the grain-inertia regime, and the transitional regime occupied the intermediate range of N.

According to Bagnold's theory, our experiment is belongs to the grain-inertia regime.

2.3.2 Some Kinetic Theory Concepts

The flow regime in which nearly instantaneous collisions are the dominant means of momentum and energy transport has been termed the grain inertia regime by Bagnold which we have learned in **2.3.1**. Bagnold argued that under these circumstances momentum transfer occurs by a succession of glancing collisions as grains of one layer overtake those of the adjacent slower layer. Both the change in momentum during a single

collision and the rate at which collisions occur are proportional to the relative velocity of the two layers. Through Bagnold's experiment, he approved that both the shear and normal stresses will vary as the square of the shear rate. This behavior was verified by several subsequent workers as Savage, Hanes, and Stadler[Savage(1989)]. We shall discuss it's physical reason dilatancy in **2.4.1**.

Bagnold's basic ideas have been extended along the lines of the 'hard-sphere' kinetic theories used for the analysis of dense gases and liquids[Savage(1989)]. Some important results that emerge are the evolution equations for the particle velocity fluctuations and spins. The kinetic energy associated with the translational velocity fluctuations has been related to the 'granular temperature', which has an obvious analogy with the definition of the temperature in a fluid at the molecular level.

It is recognized that one of the important aspects in the analysis of shear flow is the treatment of boundary conditions, both at a free surface and next to a solid wall.

2.4 Some Other Important Physical Concepts

2.4.1 Dilatancy

This is a concept to describe the property possessed by a mass of granular material to alter its volume in accordance with a change in the arrangement of its grain. During this quasi-static deformation, dilatancy is a consequence of kinematic restrictions. However, under rapid shearing conditions analogous things occur. In Bagnold's simple grain inertia model it was found that the normal stress(which Bagnold termed the dispersive stress) increases with the square of the shear rate. Hence, during shearing motions, the development of

these stresses will tend to expand the thickness of the shear layer. For this reason sheared granular materials are sometimes termed 'dilatant' materials. Because in the initial state the spherical grains are closely packed, when the bulk is sheared, particle overriding and a vertical expansion occurs. Reynolds used these ideas about dilatancy to explain a phenomenon which can be observed when walking along the seashore. When one's foot is planted on the moist sand, shear and dilation occur and the area around the foot immediately becomes dry. But, when the foot is raised, water is drawn in to occupy the additional voids created and a pool of water soon collects in the foot print.

2.4.2 Internal Friction Angle

There is an important distinction between granular material and fluid. That is granular material can be piled in a heap while fluid can not. For a given granular material the free surface can be inclined at some maximum value corresponding to the material's *angle of repose.* This behavior is similar to the sliding of a block on an inclined rough plane which will occur when the inclination angle is greater than the friction angle. Analogous things occur in the interior of a slowly deforming granular material. For a cohesionless material, the behavior is well described by the Mohr-Coulomb yield criterion[Savage(1989)], which states that yielding will occur at a point on a plane element when

$$|\tau| = \sigma \tan\phi \qquad (2\text{-}2)$$

where τ and σ are respectively the shear and normal stress acting on the element, and ϕ is the internal friction angle.

This condition is satisfied in $\tau - \sigma$ space [Savage(1992)] for the simplest case of a cohesionless material with a constant internal friction angle ϕ as shown in **Figure 2.1**.

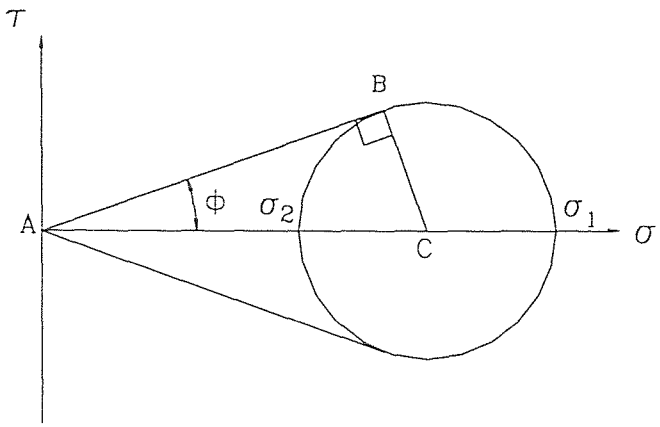

Figure 2.1 $\tau - \sigma$ Space for the Simplest Case of A Cohesionless Material with A Constant Friction Angle ϕ

Note that the ratio of the major principal stress σ_1 to the minor principle stress σ_2 can be expressed in terms of the friction angle ϕ as

$$\frac{\sigma_1}{\sigma_2} = \frac{(1+\sin\phi)}{(1-\sin\phi)} \qquad (2\text{-}3)$$

2.4.3 Large Energy Dissipation

During rapid flows the particles are in a highly agitated state, continually colliding with one another. Since the particles are inelastic and frictional, the kinetic energy associated with the velocity fluctuations is dissipated with each collision. Granular systems are extremely dissipative and in the absence of some driving mechanism, the fluctuations very quickly die away. This sizable energy dissipation is one major difference between granular

flows and gases at the molecular level. In the case of the granular material, energy can be degraded one level low, the kinetic energy of the particle fluctuations is transformed, resulting in an increase in the temperature of the individual grain. One means of maintaining the velocity fluctuations in a mass of granular material is to supply energy by vibrating a wall of container.

2.4.4 Granular Reynold Number

Let us consider the case of a simple granualr shear flow that might be generated by the relative velocity U between two rough parallel plates spaced a distance H_s apart. We can express the shear stress as $\tau = \mu_{eff}(U/H_s)$ where μ_{eff} is the effective viscosity of the sheared granular material. Consequently we can define a granular Renolds number for this flow as

$$R_{eG} = \frac{\rho U H_s}{\mu_{eff}} \qquad (2\text{-}4)$$

where $\rho = \rho_p \nu$ is the bulk density, ρ_p is the mass density of the individual particles, and ν is the solid volume fraction(volume of solid/total volume)[Savage(1989)].

2.5 Flow Mode and Dimensional Analysis

As we mentioned in 2.3.1, our experiment belongs to the grain-inertia regime in which the Bagnold number N is greater than 450, which is also named as dry cohesionless granular materials flow.

During the deformation of a bulk or dry granular material, mean stress may be generated by a number of different mechanisms. In general, the instantaneous motions of particular grains, their tranlational velocities and spins, are different from the mean motion of the bulk. Individual particles may interact with one another in various ways; in rigid clusters of particles which generate a network of contact forces through sustained rolling or sliding contacts, or by nearly instantaneous collisions during which linear and angular momentum are exchanged and energy is dissipated because of inelasticity and friction. The relative importance of these mechanisms may be used as the characteristics which define various flow regimes. Some insight into the functional dependence of the stresses on the flow and material properties may be obtained through dimensional analysis. It is convenient to work in terms of the deviatoric stress $\tilde{\tau}_{ij}$ and mean normal pressure p. They can be expressed as

$$\tilde{\tau}_{ij} = f_n[\rho_p, u_{1,2}, (\upsilon^2)^{1/2}, p, \nu, d, H, g, e, \mu, E, s] \tag{2-5}$$

and

$$p = f_n[\rho_p, u_{1,2}, (\upsilon^2)^{1/2}, (\omega^2)^{1/2}, \nu, d, H, P_B, g, e, \mu, E, s] \tag{2-6}$$

where $u_{1,2}$: the components of the velocity gradient,

ρ_p : the mass density of the individual solid particles,

$(\upsilon^2)^{1/2}$ *and* $(\omega^2)^{1/2}$: the root mean squares of the translational and rotational velocity fluctuations arising from interparticle collisions.

P_B : some reference or characteristics value of the normal stress applied at the boundary of the sheared region,

ν : the solid fraction(volume of solid ÷ total volume),

d : the particle diameter,

H : the length scale for the width of shear flow,

g : the gravitational acceleration,

e : the coefficient of restitution,

μ : the surface coefficient of friction,

E : the modules of elasticity of the solid particles,

s : the shape factor defining the angularity or sphericity of the solid particles.

We do not discuss the details of equation f_n here. But please firstly notice that the pressure p has been included in the functional relationship for $\tilde{\tau}_{ij}$ to explicitly recover the dependence of shear stress or normal pressure, secondly we can know from (2-5) and (2-6) that the most important and critical variables which is difficult to get because of its motion characteristics is the υ *and* ω, the translational and rotational velocity in the movement. All the other variables can be got from derivative, calculation, measurement or handbook.

We shall use the dimensionless number to get rid of the influence of different circumstance and dimension. That will appear in the following chapters.

2.6 Flow in Inclined Chute

Many industrial processes that involve the transportation, handling, and storage of granular materials make extensive use of devices such as dins, hoppers, channels, and inclined chutes. We shall focus on chute flow here.

Some studies of flows in inclined chutes have been directed toward the solution of some problems such as:

- to determine flow rates.
- to determine the optimum profile and cross section of curved chutes for the transport of granular materials.
- to obtain a better understanding of the mechanics and constitutive behavior of granular materials.

The steady, two-dimensional, free-surface flow down a tough inclined plane can be regarded as a simple viscometric flow. For such a flow down a plane inclined at an angle θ to the horizontal (**Figure 2.2**),

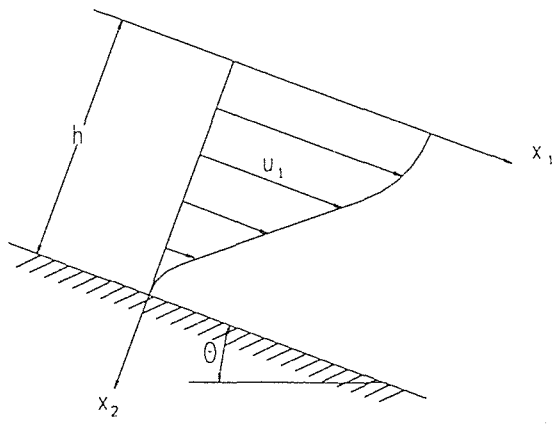

Figure 2.2 2D Simple Viscometric Flow

the normal and shear stresses on a plane parallel to the bed are given by the momentum equations as

$$\tau_{22} = \cos\theta \int_0^{x_2} \gamma \, dx_2 \qquad (2\text{-}7)$$

$$\tau_{12} = \sin\theta \int_0^{x_2} \gamma \, dx_2 \tag{2-8}$$

where the bulk-specific weight $\gamma = \rho_p v g$, thus

$$\tau_{12} / \tau_{22} = \tan\theta = const \tag{2-9}$$

throughout the depth.

For such a flow to exist, the constitutive behavior of the granular material, in particular the dynamic friction angle ϕ_D, must be consistent with equation (2-9).

For beds that are made fully rough (for example, by fixing a layer of particles to the bed) no flows are possible for values of θ less than the angle of repose for the granular material.

For bed that is not roughened, or is partially roughened, flow will begin when θ exceeds the wall friction angle, which is related to the coefficient of friction between the bed granular material. Further increase in θ usually results in accelerated flow, but this matter is not settled and there may be a small range of bed slopes which permit nonaccelerating flows.

As a factor, the chute sidewall friction is also important in the flow that even if the flow was two-dimensional and sidewall slip occurred, the sidewall friction could still exert a restraining influence on the flow. Because the pressure increased with depth, the sidewall friction increases with depth, tending to decrease the velocity near bed from what might occur in the absence of sidewall friction.

Up to now, many kinds of chute flow experiments have been done by some scientists. Some differences between the velocity profiles measured by various research appear in their results. The essential explanation for the different kinds of velocity profiles

observed seems to be that there are a number of different flows. And usually three distinct types of flow patterns are accepted [Savage(1984)] in this kind of dry flow as following:

(I) *Immature sliding flow*

In this case the bed slope θ is close to the angle of repose of the material. There can be a stationary layer just on top of the bed, thicker on the upstream than on the downstream side. In other words, an effective(or zero-velocity) bed surface occurs within the material itself, its slope being greater than the slope of the solid plane surface of the actual channel. The velocities near the bed are quite low. The flow is probably in the transitional regime between the quasi-state and the grain-inertia regime.

(II) Sliding flow

For a slightly increased bed slope, there is no dead region next to the channel bed, all the particles are in motion, the shear rate approaches a constant value over the depth, and the velocity approach the straight linear distribution[Savage(1984)]. The flow is probably approaching the grain-inertia regime. The free surface is fairly distinct, saltation of particles may be present, but individual particle jumps are not large.

(III) *Splashing flow*

With a further increase in bed slope the velocity profile becomes blunter, with a higher shear rate near the bed than near the top of the flow. Saltation is vigorous, and the top of the flow consists of a low-density cloud of particles rather than a distinct free surface. The motions of the saltating particles and those near the upper layer are affected fluid drag.

CHAPTER 3

EXPERIMENTAL SETUP

3.1 Overview

The block diagram, **Figure 3.1**, shows the concept of the experimental setup which is composed of one fundamental flow cycle, two alternative boundary conditions, and three main testing means.

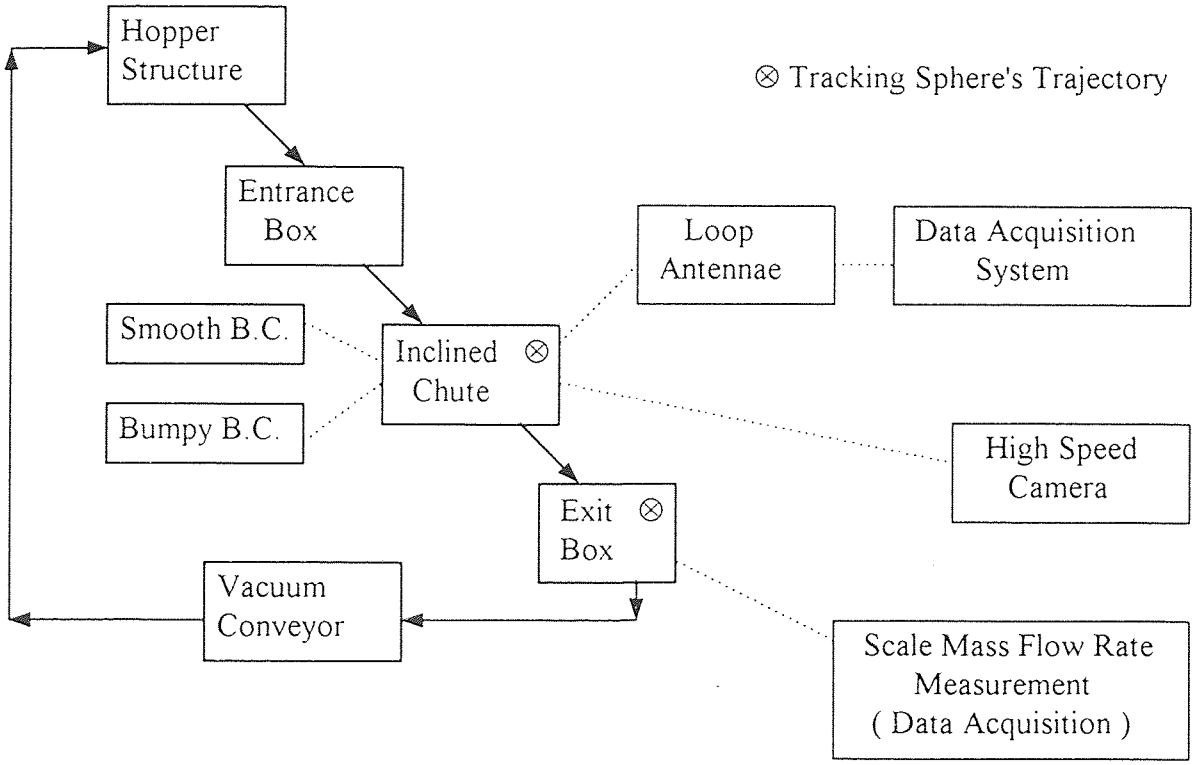

Figure 3.1 Experimental Setup Block Diagram.

The sphere flow cycle starts from hopper when the hopper gate is opened. The flow then enters the entrance box, passes through the chute gate space(a certain height sluice), and continues along the 120 inch long chute, which is tessellated with 27 loop antennae. The flow does not stop until it reaches the exit box set on the top of an electrical scale. After the hopper is emptied, the flow spheres are transported back to the hopper using a pneumatic or vacuum conveyor system to prepare for another experimental cycle.

The tracking sphere with three transmitters, battery, and circuit board housed inside will be injected into this flow as an ordinary sphere but its trajectory can be determined with the particle tracking system. This tracking technique has been developed in Particle Technology Center at New Jersey Institute of Technology and will be introduced in **Chapter 4**.

There are three main testing means do the calibration in the experiment: Data Acquisition System works after it is connected to the loop antennae through electronic circuit system; High Speed Camera can record either the flow velocity of the sphere bulk surface or the flow speed at the side walls; Mass Flow Rate Measurement (Data Acquisition) is connected to the scale DW 800 High Accuracy Digital Weight Indicator through RS-232 interface.

Figure 3.2 is a photo of the chute system. The hopper and vacuum system can not be seen completely from the picture because they errect out of the ceiling opening.

In what follows, descriptions of the chute system's individual components are given. Some details such as design purpose and main dimensions will be introduced.

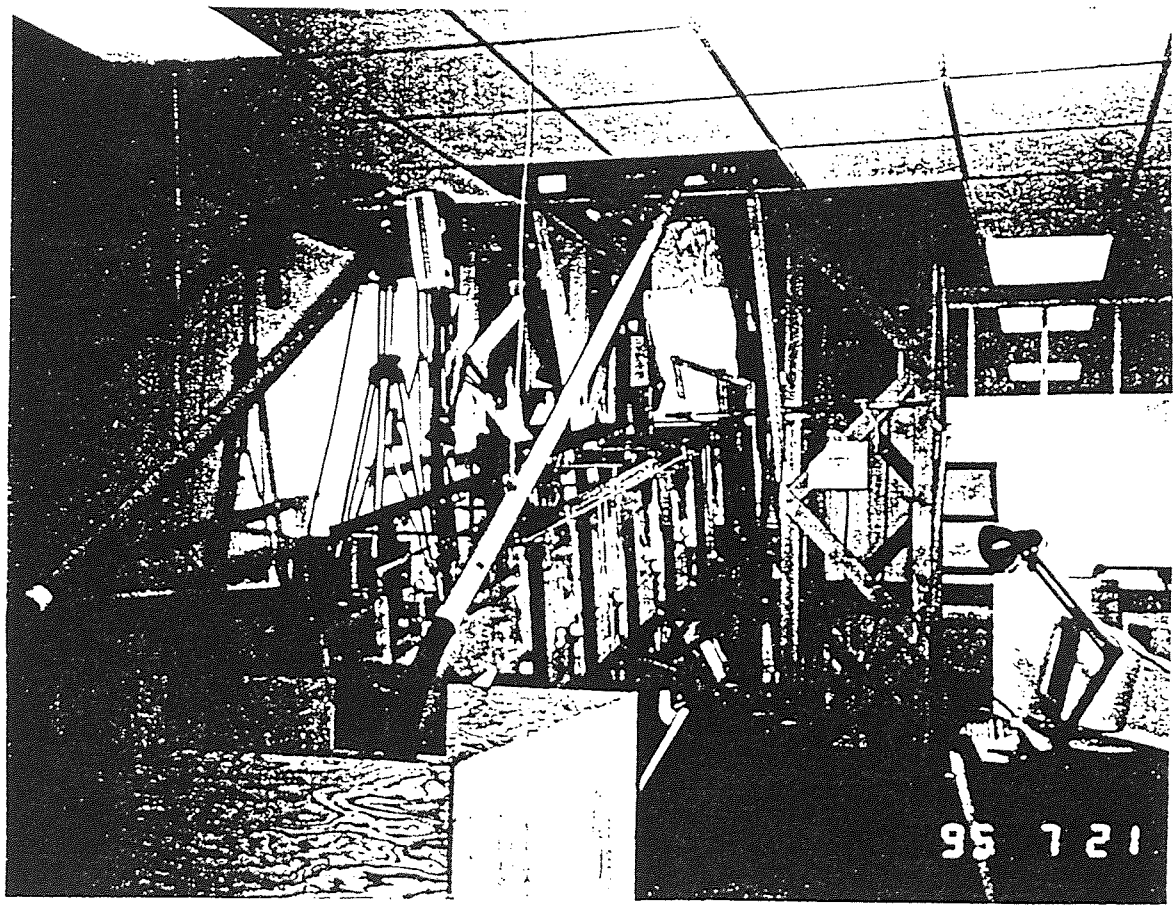

Figure 3.2 A View of Experimental Setup

3.2 Chute

The inclined chute is 10 feet long with an variable inclination angle from 0 degree to 25 degrees, an adjustable width from 5 inches to 14.5 inches, and an flexible sluice entrance gate which can open from 0 to 9 inch height. The structure of the chute and the global coordinate system are shown in **Figure 3.3**.

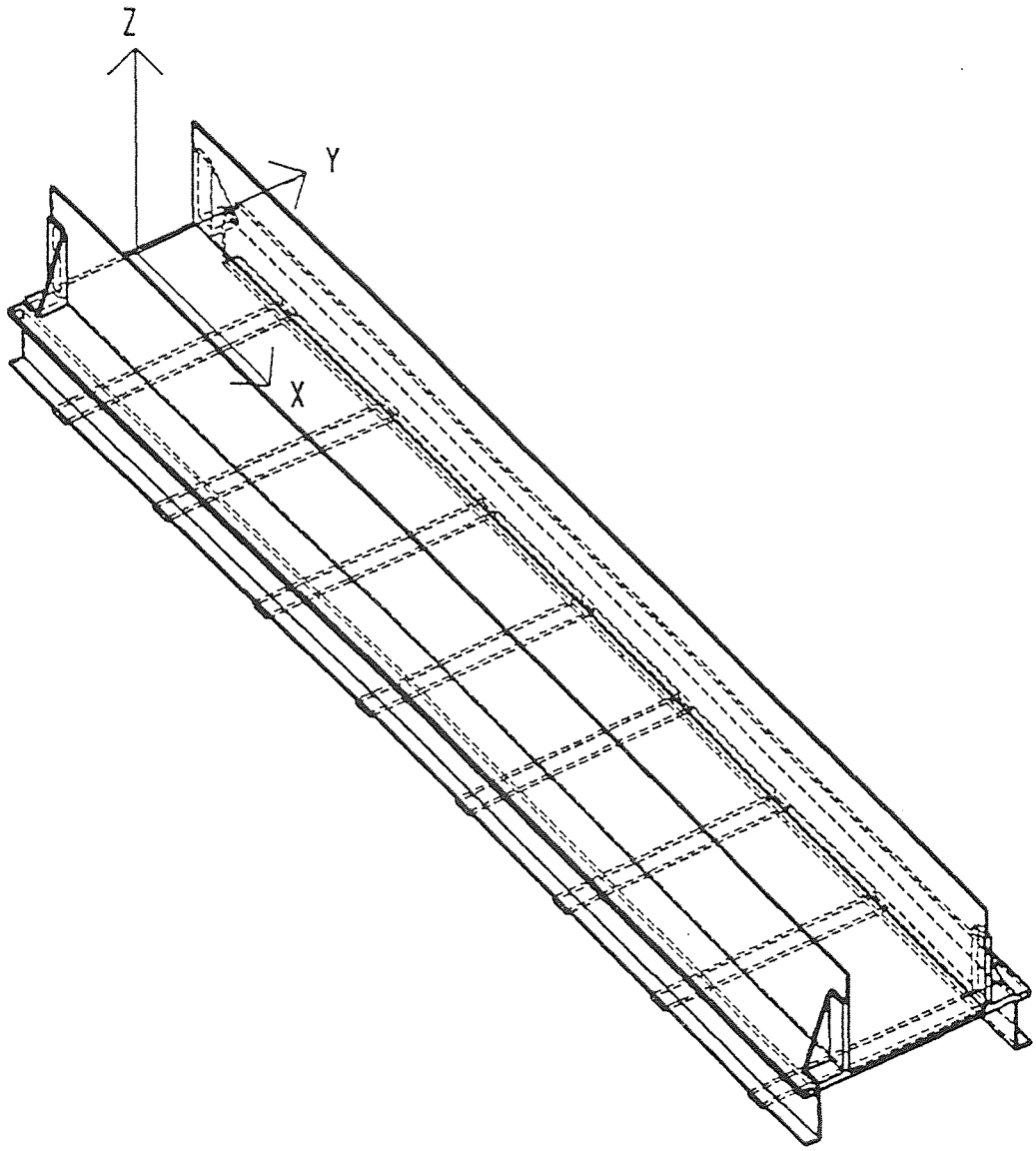

Figure 3.3 Chute

The chute is fabricated from "radio-transparent" materials, i. e., acrylic sheets and Extren 500 and 600 of various structural shapes. This is necessary for the particle tracking system which is based on magnetic induction. It is fastened together by nylon and extren nuts and bolts. The only metallic components of the structure are the square and rectangular loop antennae that tessellate the chute. See **3.7** Antennae and Their Support System for the detail.

The floor of the chute is exchangeable. We can use either acrylic clear plane sheet or clear prismatic sheet as the bed surface to build smooth or bumpy boundary conditions. The same change can be made on two side walls of the chute.

3.3 Hopper

The hopper can hold up to 36 cubic feet and has a variable discharge area to a maximum of 17 × 17 square inches. The discharge area is controlled by the hopper gate opening operation. The storage volume of hopper, 36 cubic feet, is more than 3 times maximum chute flow volume, 4.5"×120"×9"= 15,660 $cu-in = 9\ cu-ft$. Usually, we take 3 times the chute flow volume as the enough preparation volume to show the steady flow period in the experiment.

For the purpose that hopper can continuously supply spheres to the chute flow in various experimental conditions, the hopper is so designed that its main flow angle is 26 degrees which is larger than the maximum inclination angle of the chute(25 degrees) and its maximum discharge area, 7"×11.7", is greater than the maximum sluice area of the chute, 4.5"×9", which is controlled by the chute gate opening extent.

Like the chute, the hopper has symmetrical speed space to the flow direction and this symmetry forces a tendency towards homogeneous flow[Hanes(1991)].

Figure 3.4 shows hopper outline. The design of the front and back sides of the hopper was determined according to the available space in the laboratory, considering the other system components.

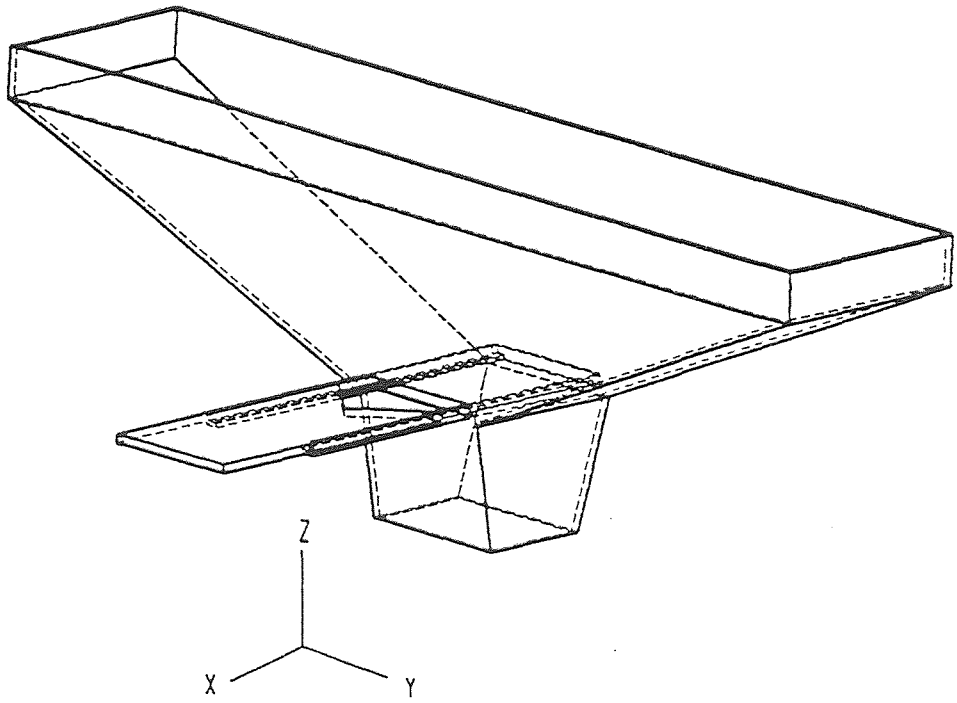

Figure 3.4 Hopper

The hopper and its support structure are made up of ordinary wood, another kind of "radio-transparent" material. The design of the support structure was undergone the safety calculation which is based on the allowable stress in Merritt "Building Design and Construction Handbook". The hopper can be sealed well enough so that it can be used as a large vacuum drum. We will introduce this section in 3.6, "Vacuum Conveyor System".

3.4 Exit Box and Scale System

The exit box constructed of wood with a volume of 45 cubic-feet is seated on top of a platform scale which is connected to the weight indicator and computer. They are shown in **Figure 3.5**.

The exit box is constructed of wood plates to avoiding influence to the radio-magnetic field of the tracking system.

The scale has a 3,500 lb. capacity(The capacity was changed from 2,000 to 3,500 through changing the scale's program by the service man of Sterling Scale Company after some experiment trying in our lab.), 0.5 lb. graduations in reality(in manual, it is described as 0.2 graduations), and a square shape of 3'×3' by 4" high. The Sterling Model 800 Digital Weight Indicator we use has 16,000,000 internal counts with a complex digital averaging program to obtain high accuracy and stability. Up to 50,000 counts can be displayed. Keyboard calibration is standard and a special high tech filtering circuit eliminates problems caused by vibration. The scale is in the maximum calibration rate up to 10 times per second and the sensitivity 0.5 Micro Volts per graduation. On the scale,

we choose the standard bi-directional RS232C port which can be interfaced to most computers, and printers.

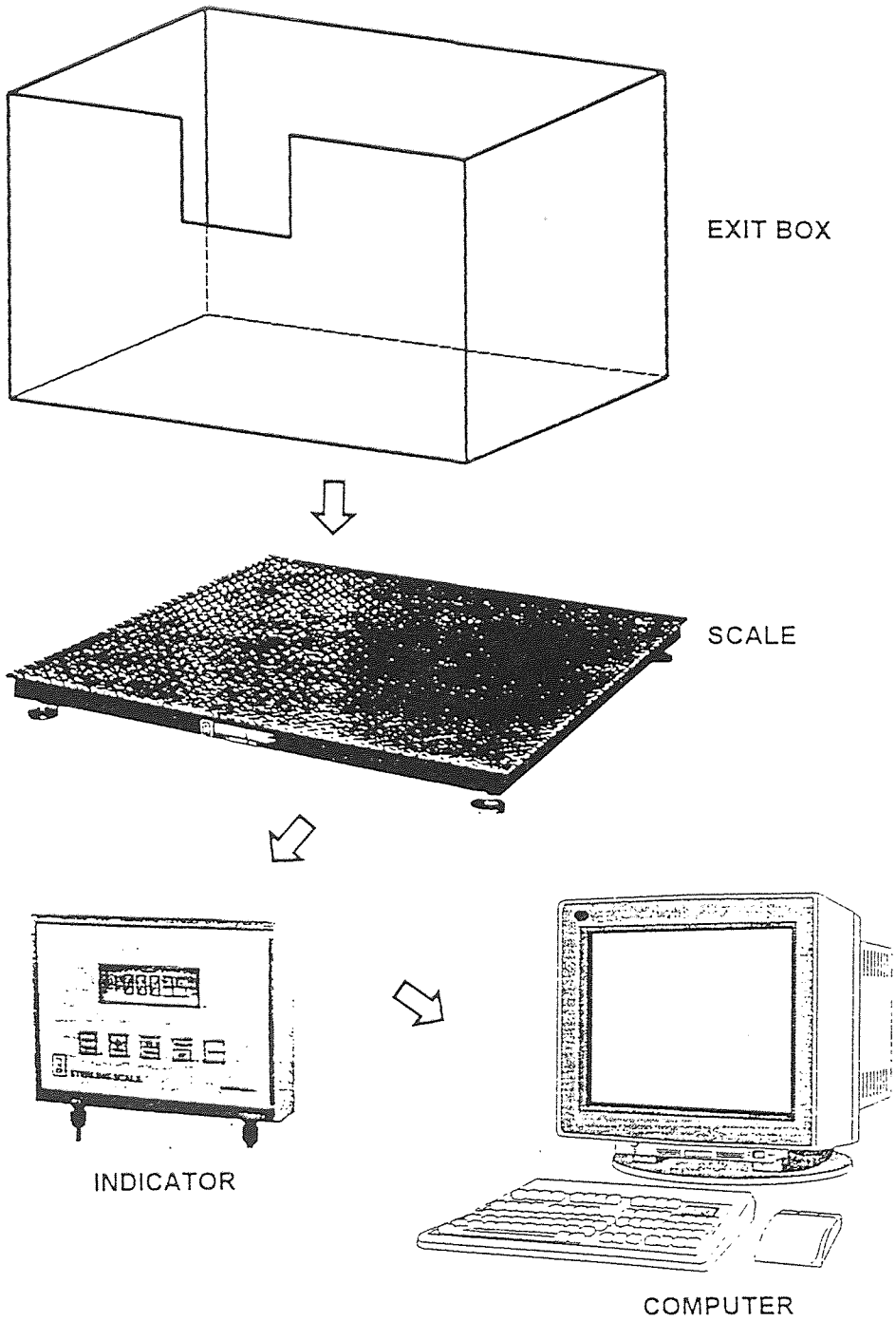

Figure 3.5 Exit Box and Scale System

3.5 Vacuum Conveyor System

This system is mainly composed of the three top assemblies of the ordinary blowing wet/dry vacuums, the whole hopper storage space, and two extrusion plastic tubes extended to access the exit box through a hose.

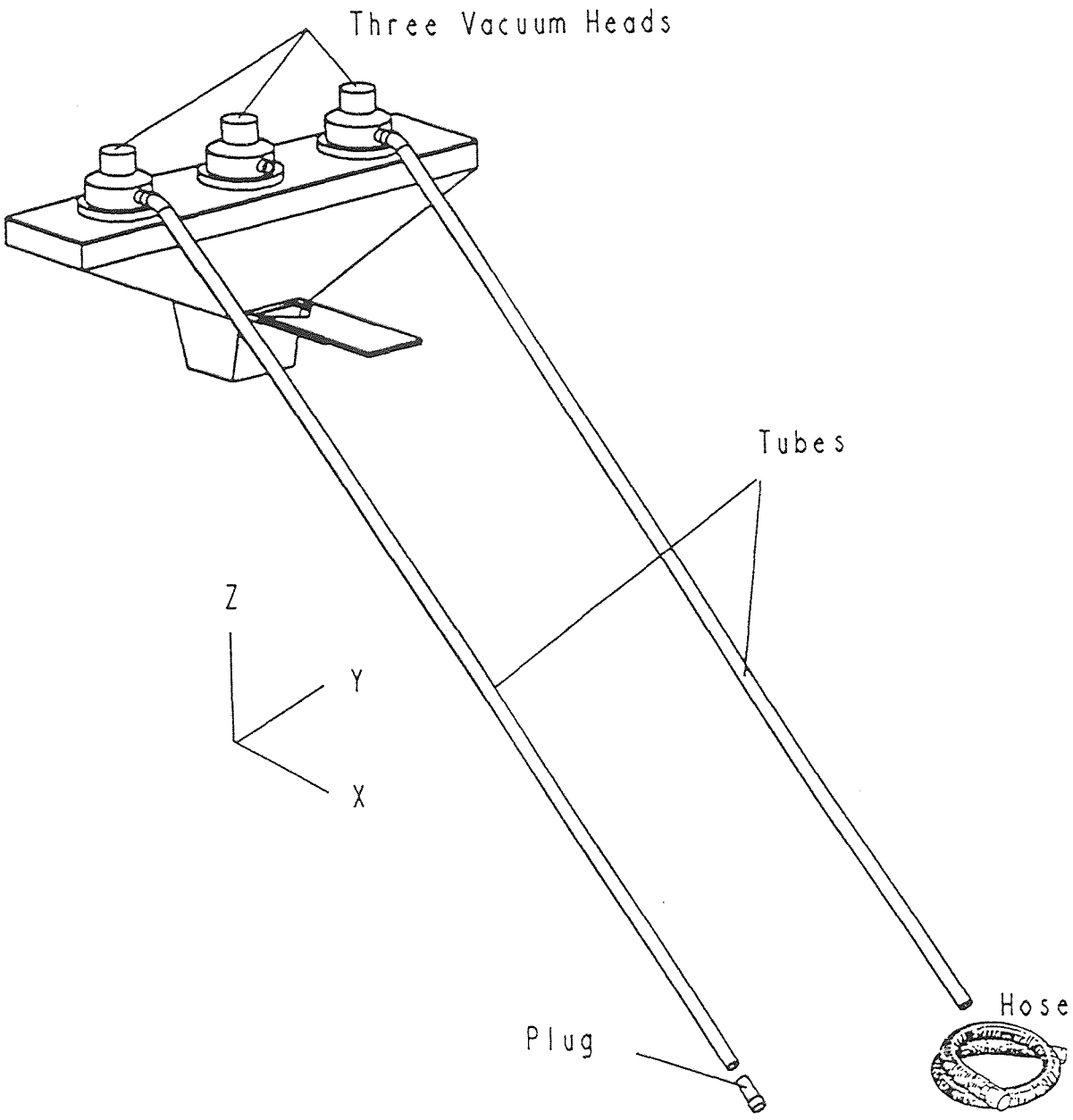

Figure 3.6 Vacuum Conveyor System

The concept of the system structure is shown in **Figure 3.6**. The three top assemblies, which are composed of a motor, blower wheel, remove the air from the sealed hopper to make it act as a very big vacuum drum. Two plastic tubes of $2\frac{1}{4}$" diameter extend to the exit box from two of three top assemblies and access the spheres in the exit box with the help of a hose. To increase the vacuum of the hopper, either of the extrusion tubes can be plugged to allow only one tube to drew up sphere from the exit box to the hopper.

3.6 Antennae and Their Support System

In the experiment, the antennae voltage generated are used to compute the path and angle of the tracking sphere. The presence of an electromagnetic source, i.e. three transmitters embedded in the tracking sphere, will induce a current in nearby antennae. The magnitude of this induced current will be primarily a function of the conductance of the pick-up antenna and the orientation of transmitting source with respect to the receiving antennae.

The antennae system is composed of 27 loop antennae. In it there are eleven X antennae with their 24"×24"square loop planes perpendicular to the x-axis, eight Y antennae with their 24"×32" rectangular loop planes perpendicular to the y-axis, and eight Z antennae with their 24"×32"rectangular loop planes perpendicular to the z-axis. The X , Y, and Z antennae are shown in **Figure 3.7** respectively.

The X antennae are parallel and set in 1 foot intervals each other from the entrance to the exit of the chute along the flow direction. The Y antennae lie in the plane of the chute walls, and with an overlap of 2.7" between adjacent loops. The Z antennae are

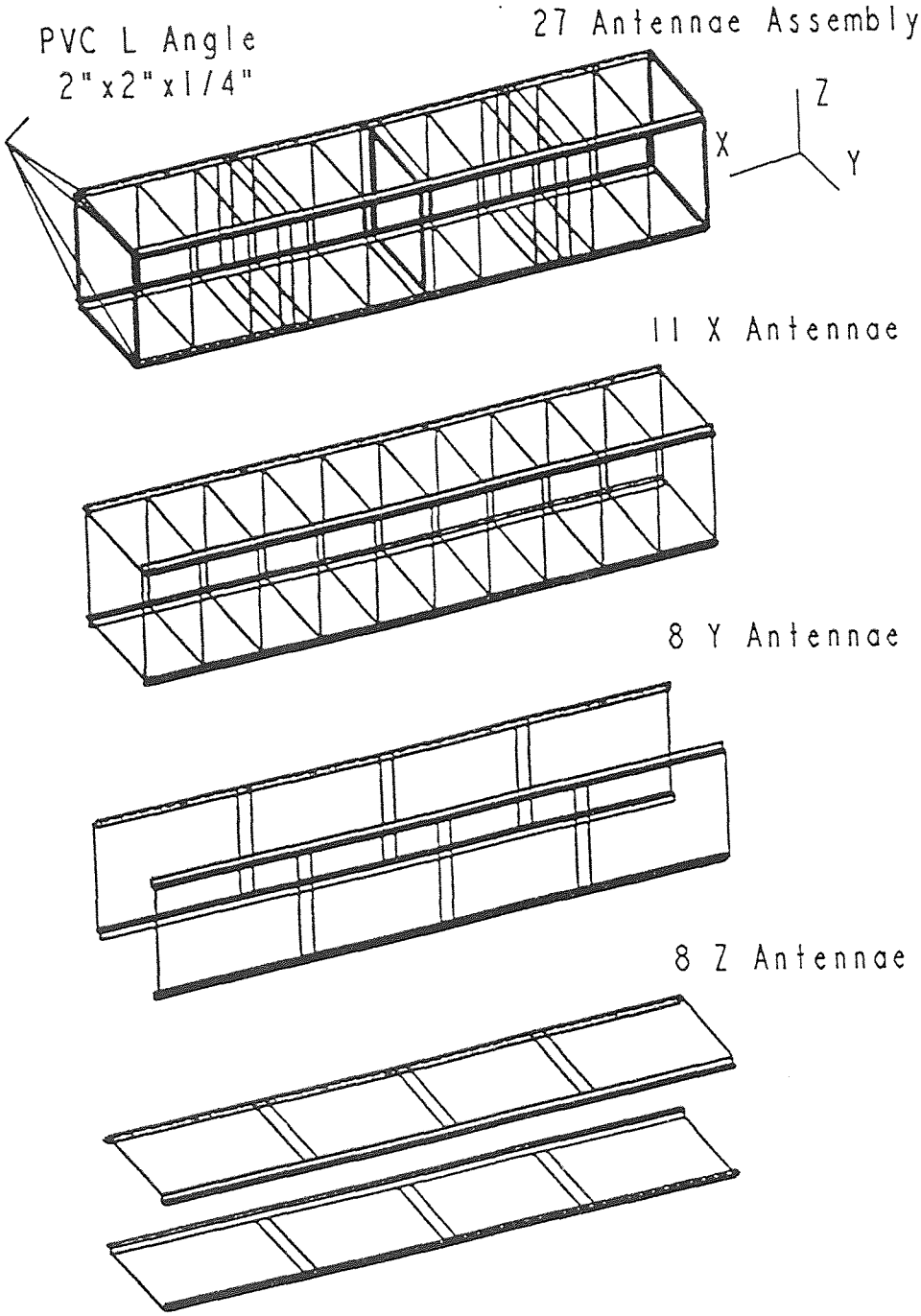

Figure 3.7 Antennae and Their Installation

arranged in a similar fashion in the upper and lower xy planes.

The antennae support system is made up of PVC equal-leg angle material to maintain the parallel distance between wires are greater than 1 inch. The support system is fasten by nylon and extren nuts and bolts. The antennae loops are made of Hoop-up Wire Yel Stranded 22 HWG.

3.7 Spheres and Tracking Sphere

In the experiment, the flow particles are 1 ± 0.002 inch diameter solid, high density polyethylene spheres ($m = 0.00757kg = 0.01669lb$). The choice of this material was made to match the size of the tracking sphere, although other flow materials can be used in future experiments. For the current system, approximately 60,000 spheres are used having a bulk weight of approximate 1,000 lb. Through the simple certain box measurement and calculation, the sphere volume fraction (Volume of Spheres/Space Occupied) is considered as 0.57.

The tracking sphere is constituted of case and transmitter assembly. The case is made up of two bored hollow halves of a 1" high density polyethylene sphere typical of those in the flowing mass. The transmitter assembly is tried to be positioned in the case that the tracking sphere's dynamic balance is the same as an ordinary flowing sphere's. The details about the principle and working procedure will be described in **CHAPTER 4**, Particle Tracking Technique.

3.8 Other Apparatus and Sets

Figure 3.8 shows the components of the Kodak Ekata Pro 1000 high speed camera system, which is mainly composed of imager, keypad, processor, monitor, cassette, and intensified imager controller.

This high speed camera system can operate in the speed from 30 to 1000 frames/second, and is valuable in optically tracking sphere on the flow surface and sidewalls.

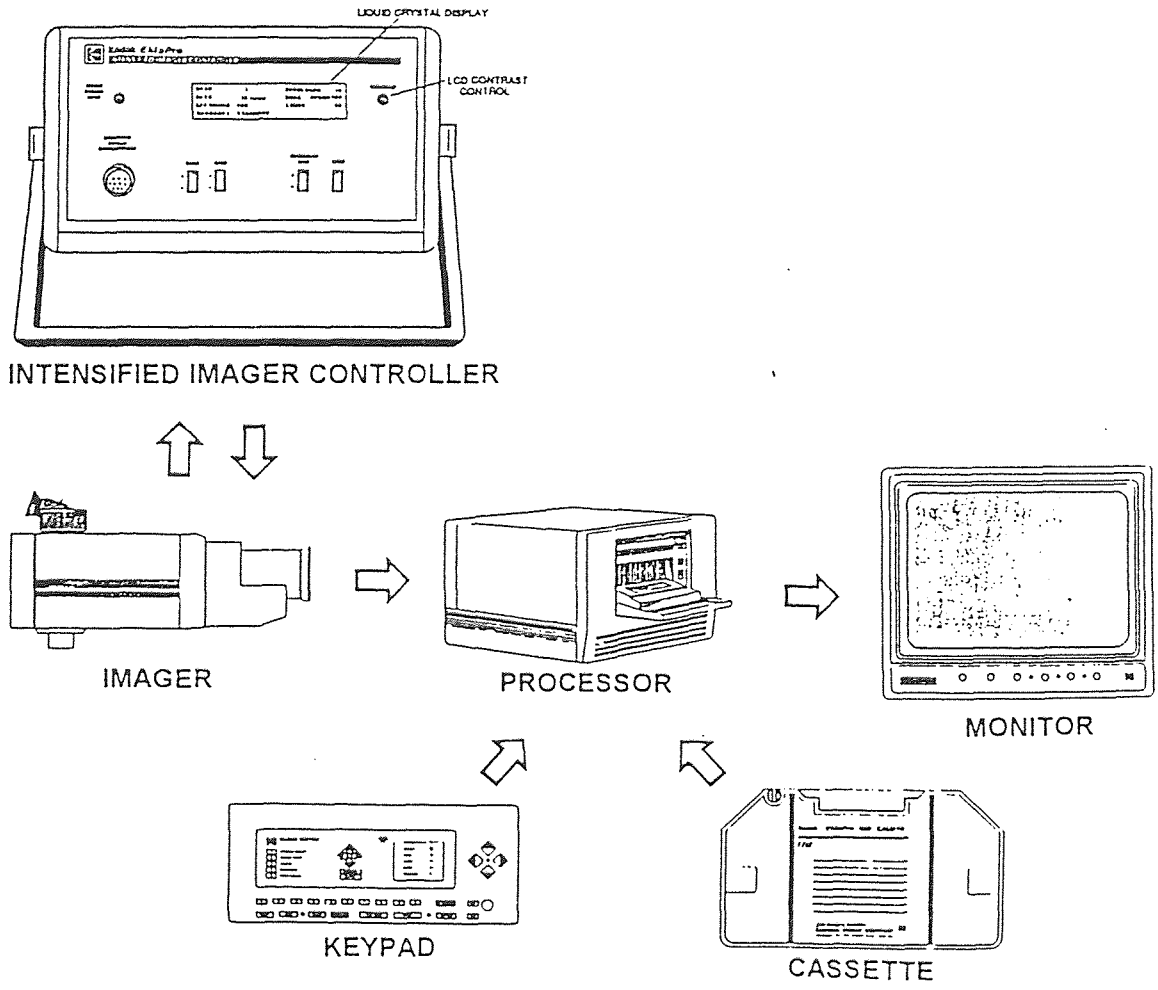

Figure 3.8 High Speed Camera System

Tracking sphere injection mechanism can introduce the tracking sphere into the flowing mass near the entrance gate. It is depicted in **Figure 3.9.** The battery in the tracking sphere is energy limited and we have to use this set to shorten the time between switch on and off time controlled by light switch(which we will introduce in **CHAPTER 4** in detail).

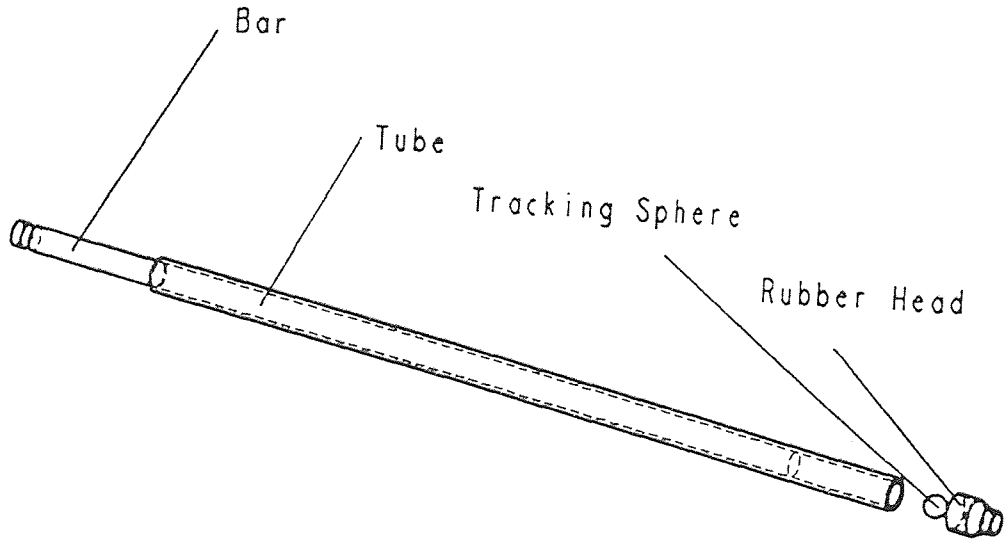

Figure 3.9 Tracking Sphere Injection

CHAPTER 4

PARTICLE TRACKING TECHNIQUE

4.1 Principle and Objective

The tracking technique is based on the principle of magnetic induction coupling. This principle states that the presence of an electromagnetic source will induce a current in nearby objects. The magnitude of this induced current will be primarily a function of the conductance of the pick-up objects and the orientation of the transmitting source with respect to the receiving objects. Objects with high conductance or low resistance include metals like copper, iron, steel, silver, gold, aluminum and so on. These metals are good receptors of electromagnetic radiation and produce currents that can be measured by readily available electronic circuitry. On the contrary, objects with low conductance like plastic, glass, wood and other non-metal ones are classified as "radio-transparent" materials or high resistance materials because the currents induced in these media is often undetectable small because of the high resistance feature of the materials.

Our objective is to determine the location and rotation of the tracking sphere using this tracking technique and to analyze the behavior of flow materials in the chute flow movement.

The fundamental physical system of tracking technique is comprised of a radio-transparent flow space accompanied with number of receiving antennae. The 1 inch diameter tracking sphere with three radio transmitters embedded in the flowing mass

induces the current in the surrounding antennae. The problem, then, is now to translate the antennae voltages into positions and orientations.

Once the mechanics of the system are established, data is collected in the form of signals from the receiving antennae. These signals are filtered, amplified, digitized, downloaded and stored in a computer. The inverse solution refers to the process by which these signals are used to determine transmitter's position and orientation. Through theories of electricity and magnetism, it is possible to estimate the signal levels in a loop antennae given the position and orientation of the transmitting source with respect to the loop. However, it is difficult to obtain an inverse solution in closed form because of the complex relationship that exists between the induced signal and the location of the transmitter. Therefore, numerical methods are used to solve an over-determined system of m non-linear equations for six unknowns($x, y, z, \alpha, \beta, \gamma$), where m is the number of receiving

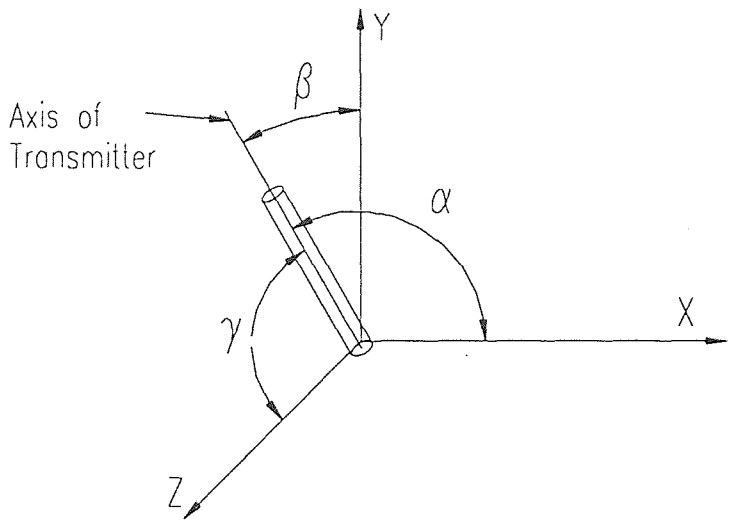

Figure 4.1 Definition of α, β and γ

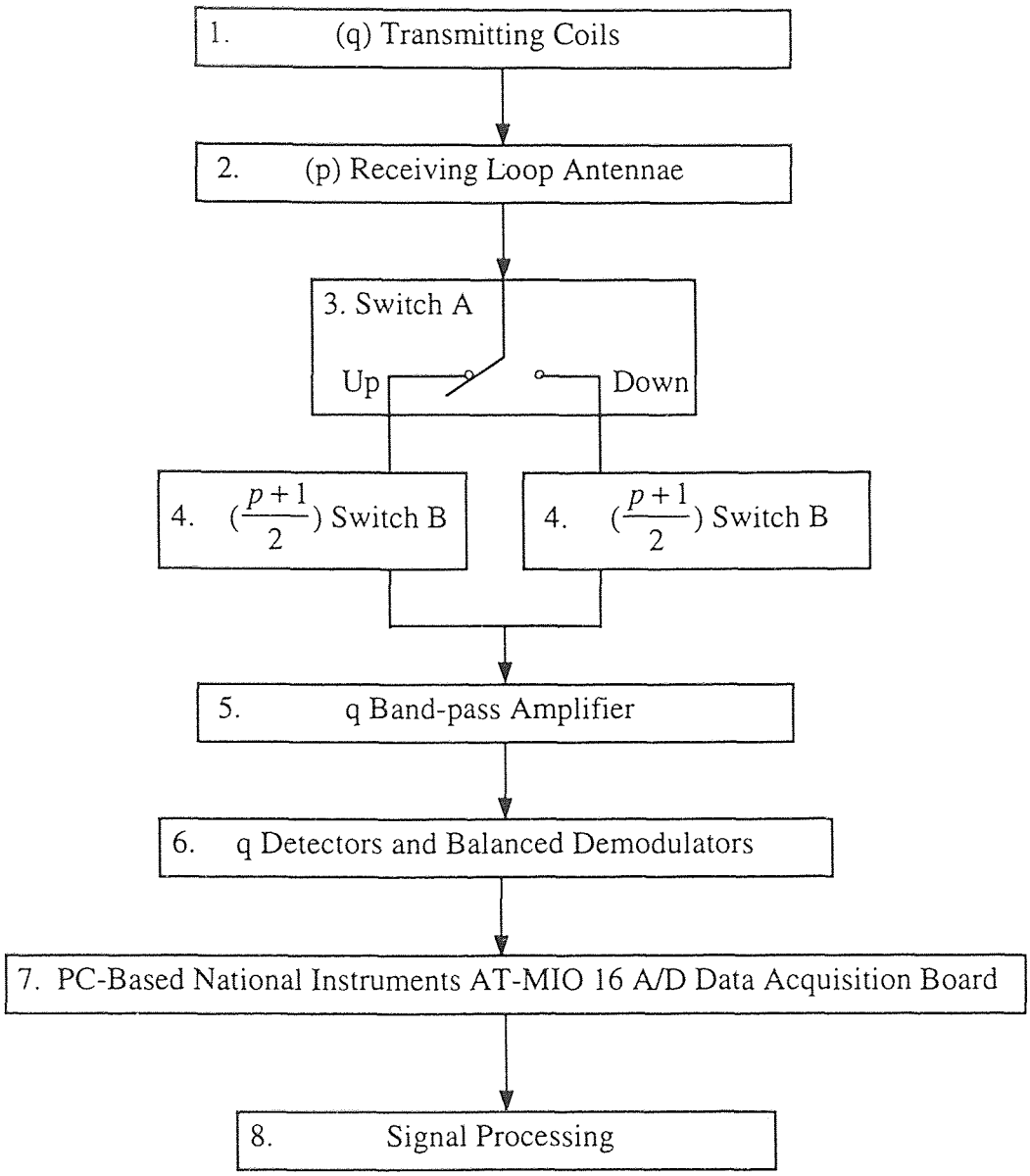

Figure 4.2 Data Acquisition Block Diagram

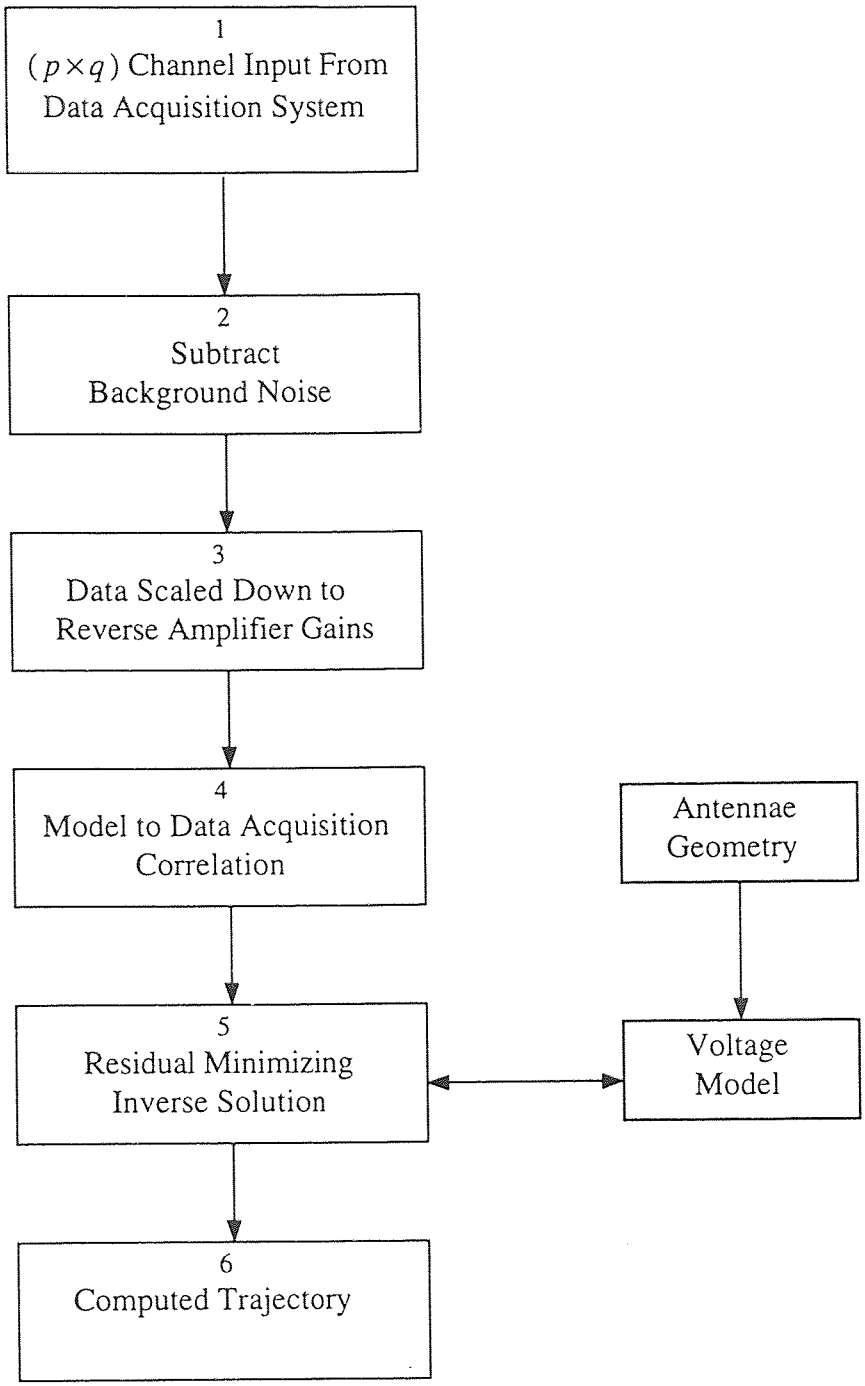

Figure 4.3 Signal Processing Block Diagram

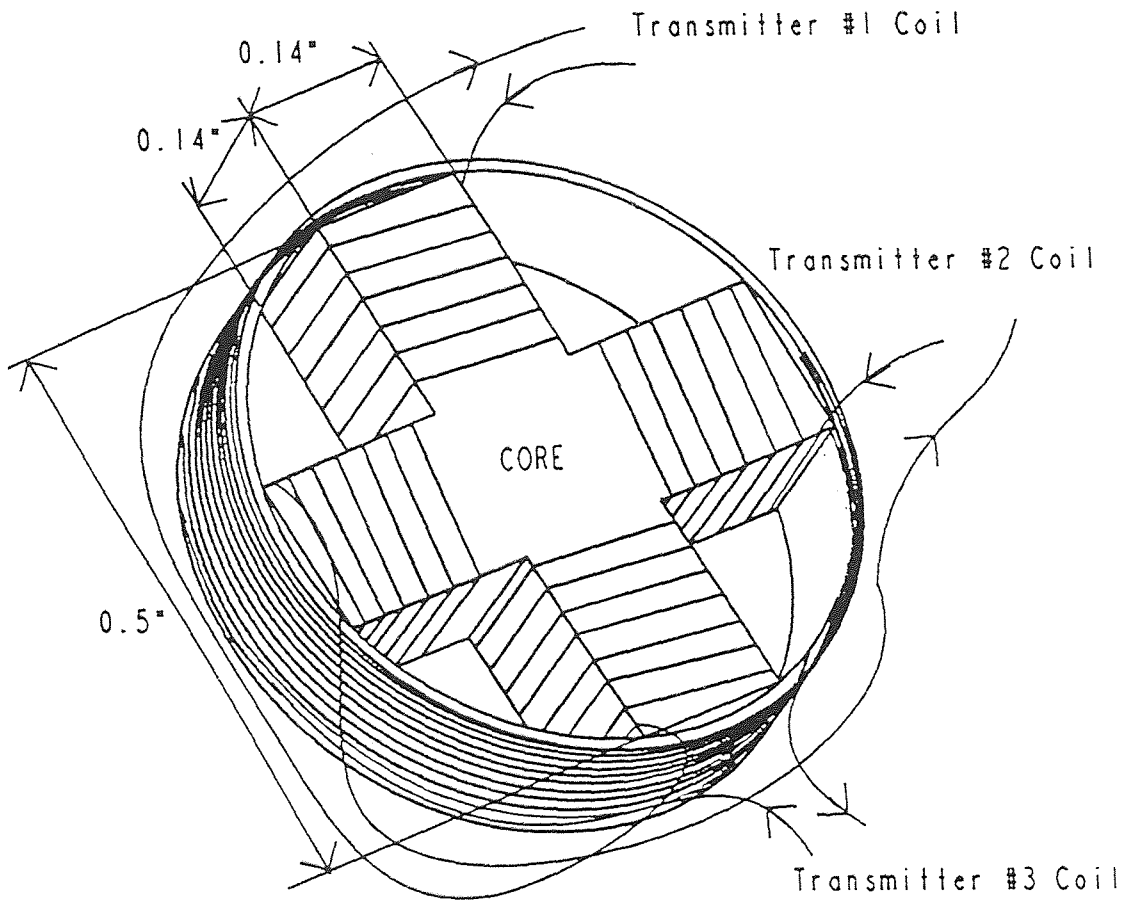

Figure 4.4 The Oscillating Coils Around the Ferrite Core

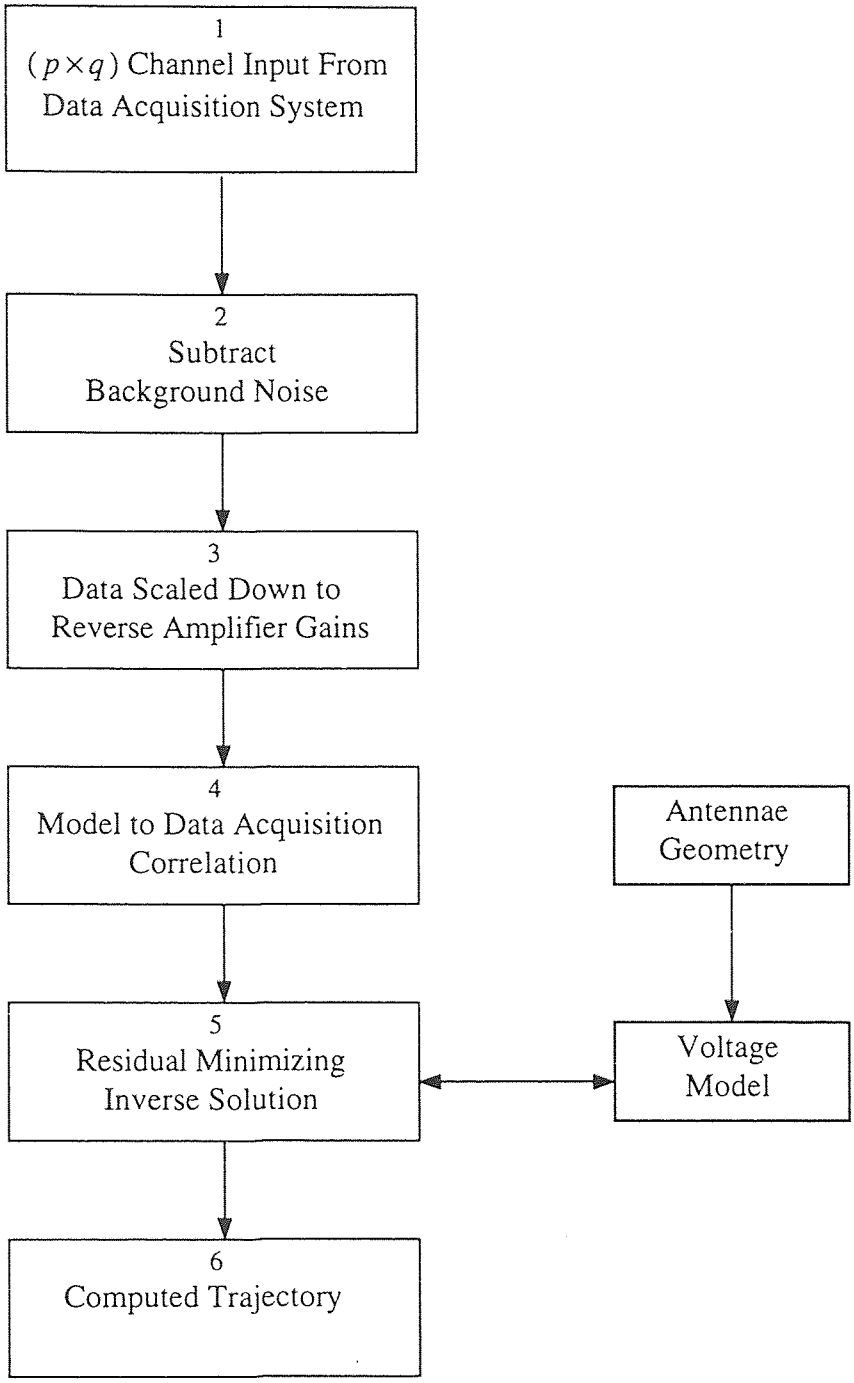

Figure 4.3 Signal Processing Block Diagram

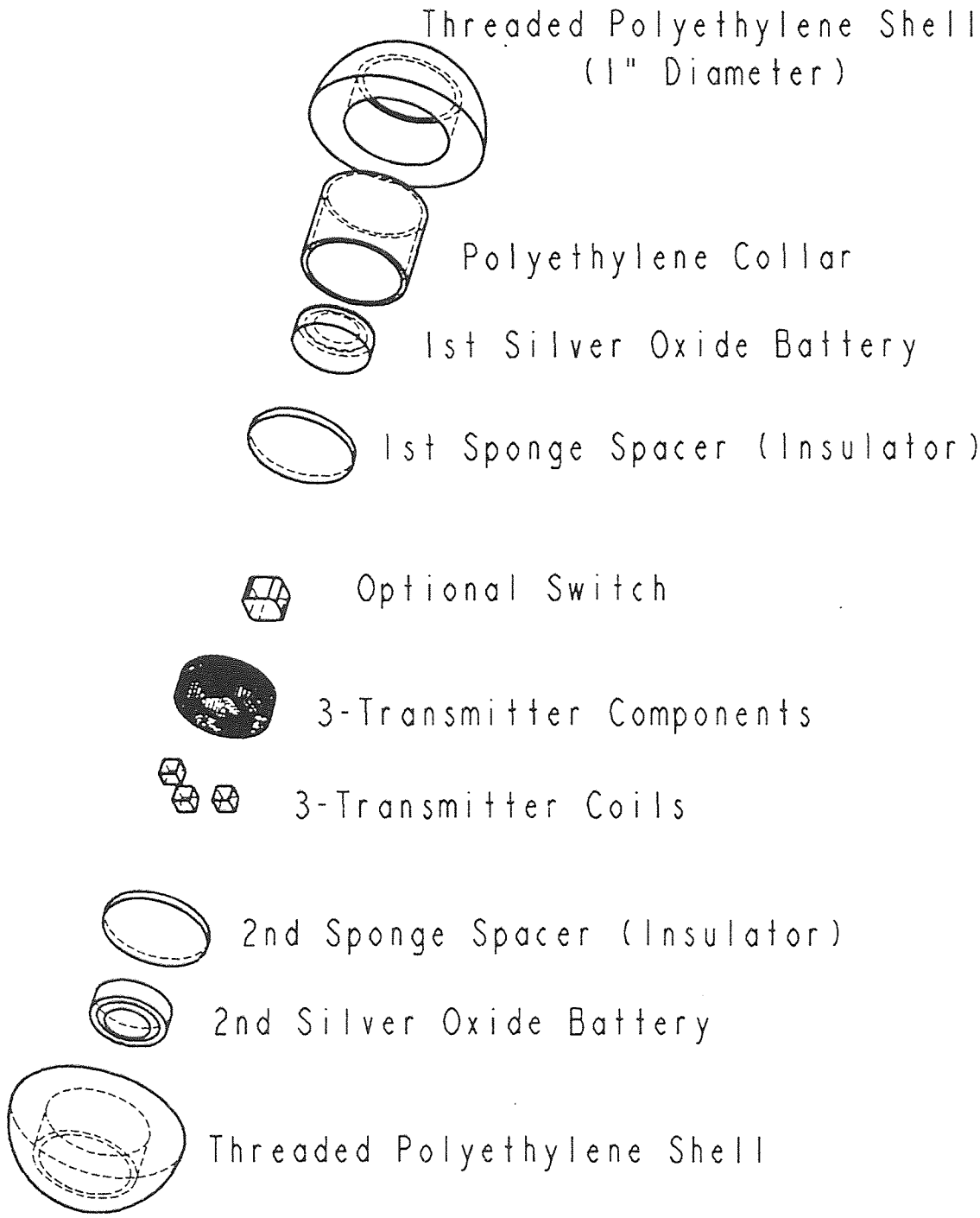

Figure 4.5 Tracking Sphere Assembly.

The required power for the circuit is provided by one 1.5 Volt nickel-cadmium battery installed as in **Figure 4.5**. It is assumed that the interference introduced by the proximity of the metallic batteries is negligible given their small size. The axes of the transmitters, as it will be discussed are defined in **Figure 4.6**. One of the transmitter circuits is shown in **Figure 4.7**.

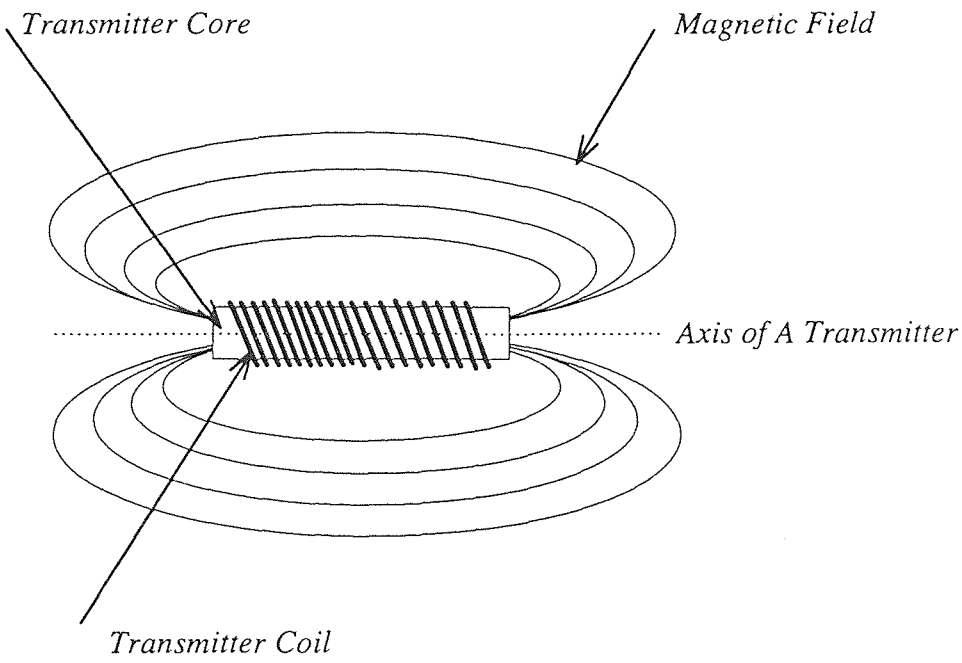

Figure 4.6 The Axis of A Transmitter

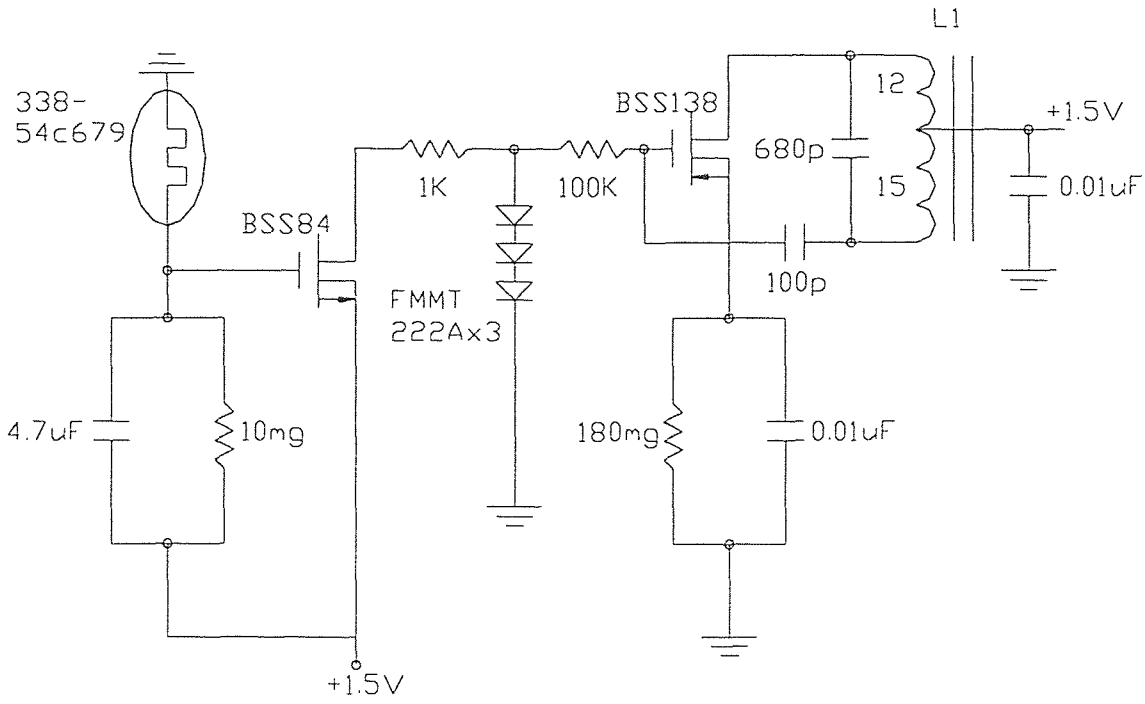

Figure 4.7 Transmitter Circuit Diagram (2.0 MHZ)

The transmitter oscillating frequencies of 2.00 MHz, 3.65 MHz, and 4.40 MHz respectively are chosen for several reasons.

From the electromagnetic theory, the higher the frequency, the more easily for receiver to pick up the signal. And the higher the frequency, the smaller the capacitance and inductance are required, subsequently, the easier the fabrication of our tracking sphere would be. However, there are some disadvantages to use a high frequency: The higher the frequency, the more difficult it is to fabricate the amplifier for the antennae receiver, and the more easily for the emitted wave to reflect back from distant metallic objects. Consequently more power will be consumed for standing these reflected waves.

Through careful analysis, we can get the first rule for choosing frequency. That is we should avoid disadvantage of high frequency while we take advantage of it. From this view the frequency should be suitable high. The second rule is we should avoid the frequencies that are frequently used in transmissions. For example, the frequencies around 1.6MHz are bad choices because they are on the MW(median wave) band of the radio and continuously in use. Also, the frequencies from 40 to 70 MHz are the low part of VHF(Very High Frequency) of the TV, 80 to 390 MHz are the high part of VHF, and 400 to 900 MHz are the UHF(Ultra High Frequency)of TV. All of these can not be chosen. Moreover, the frequency of 88 MHz on the FM(Frequency Modulation) band, is constantly in use, and represents an endless source of high power noise. Likewise, the frequency of 176 MHz is a poor choice because it is the first harmonic of the busy 88 MHz band.

The 2.00 MHz, 3.65MHz, and 4.40MHz are fairly isolated frequencies which are acceptable because they fit these two rules.

I should address here that Songyao Ren, an electrical engineer, invented a light switch for our tracking sphere and that invention solved the battery energy shortage problem for the tracking sphere in the authentic chute flow.

4.3 Antenna System

At least six antennae must be used to monitor the path of the tracking sphere because complete determination of the position and orientation of the tracking sphere translates into six unknown: three in position(x, y, z) and three in orientation(α , β , γ). That is:

$$V_{ij} = g_{ij}(x, y, z, \alpha, \beta, \gamma) \qquad (4\text{-}1)$$

where V_{ij} mean the voltage in antenna j caused by the transmitter i as a function of position and orientation of transmitter i .

The configuration of these antennae, that is their location, size, shape and number has been proved to be extremely important to the tracking system. It is found in preliminary studies that larger antennae tend to get low signals, and thus it seems, the smaller the antenna, the better the results. But, the boundary effect happens when the transmitter source very near the antenna loop circuit and that effect will interfere the result. According to electromagnetic flux theory, moreover, the more the transmitter source nears the center of antenna loop, the more accuracy the result. To avoid the boundary effect, the antenna loop size should be bigger than the area where the tracking sphere would pass and this passed area should be as centered as possible.

According to the antenna number requisition, electromagnetic flux theory, and the dimension of the inclined chute, we use 27 antenna loops on the chute(see **Figure 3.7**). The eleven X antenna loops are in 24"×24" square shape while the eight Y antenna loops and eight Z antenna loops are either in 24"×32" rectangular shapes.

The data is collected with the axis of the transmitter collinear with the axis of the antenna as the transmitter moves away from the plane of the antenna. Here, the axis of the transmitter is as defined in **Figure 4.6** and the axis of the antenna is defined as the vector of the antenna plane. The vector centered in the plane of the antenna and perpendicular to it with a magnitude equal to the area of the loop.

The position and the orientation of the antennae that cover the chute flow space also have a strong impact on the end result of the inverse solution(see **4.5**). Problems appear particularly when an orthogonality occurs between the axis of the tracking sphere's transmitter and the axis of one or more antennae. When this occurs, a very low current is induced within the antenna or antennae, resulting in a very low signal to noise ratio. In a true granular flow, such an orthongonality is rare in a sustained manner. Techniques are developed in the signal processing stage to overcome this situation. The history of the particle's path can be reconstructed by examing its position and orientation immediately before and after the orthogonality occurred and subsequently interpolating to determine a true position. But, this interpolating technique can be slightly reduced by the addition of extra antennae mounted at an angle with respect to the chute[Volcy(1994)].

The selection of antenna number is also important after the antenna number is greater than the minimum, six. To avoid coupling induction appears between parallel neighborhood wires, we have to leave enough space between antennae. But it is not desirable to use very distance antennae to compute the position and orientation of the tracking sphere because these antennae will provide low signal to noise ratios and will increase the numerical computation work without increasing the accuracy of the final results. We chose 27 antennae not only because these consideration but also because the receiver board hardware and data acquisition software limitation.

4.4 Receivers and Data Acquisition

The tracking sphere within the flow bulk yields the alternative current with only a few millivolts in the loop antennae. The receiver boards have been built to amplify these signals and isolate the 2.00MHz, 3.65MHz, and 4.00MHz transmitter frequencies. The output of these boards are positive DC voltages in the range of approximately 0 to 3 volts. It is crucial that the receiver boards amplify the signal and convert the AC input to a scaled DC voltage in a linear fashion. **Figure 4.8** is a plot of the system's linearity[Volcy(1994)].

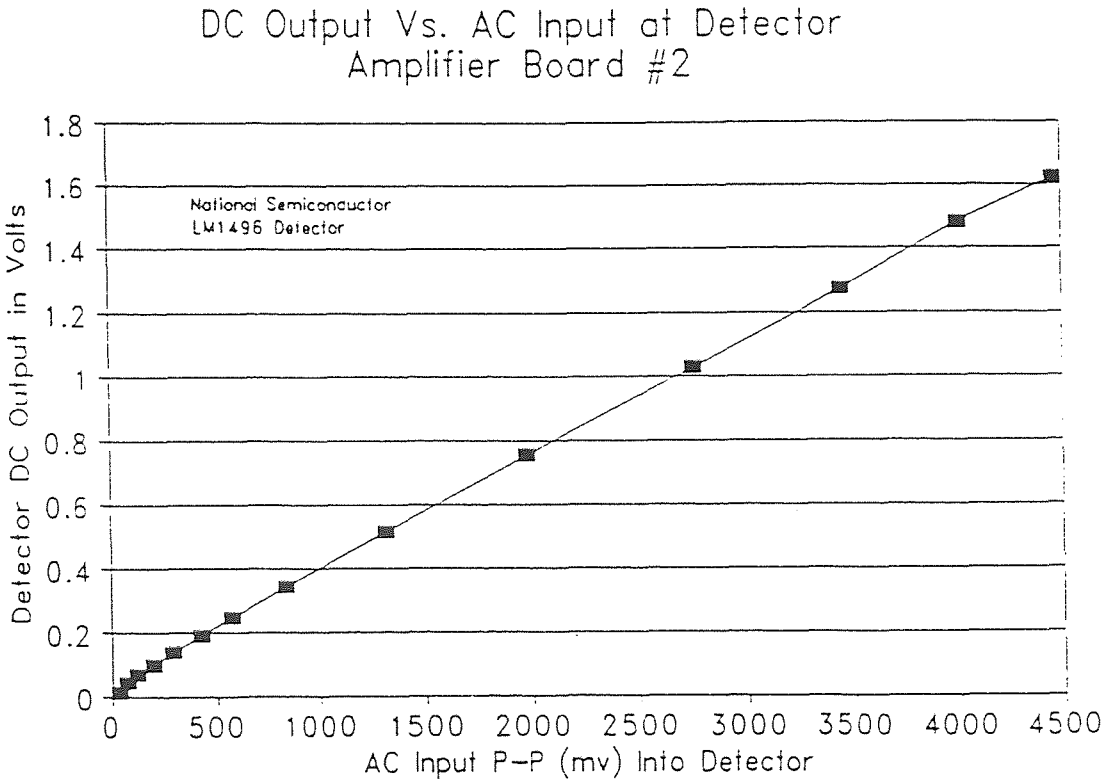

Figure 4.8 Linearity of Receiver Board at Detector Stage

The receiver boards are analogous devices and they are, in theory, sensitive to infinitesimal changes in the position and orientation of the tracking sphere. But the digital data acquisition system is sensitive to small changes in angles and positions(dependent on the transmitter's orientation with respect to the monitoring antenna). As the final results come out of digital data acquisition system, the sensitivity of the whole transmitter-receiver system is actually the sensitivity or the limitation of the digital data acquisition system.

The analog to digital system is rely on a National Instruments 12-bit Converter that outputs a value of -2047 to 2048 "counts" corresponding to -10 volts to +10volts DC.

4.5 The Concept of Signal Processing and the Inverse Solution

Immediately after the signal from the antennae have been collected, filtered, amplified, and processing to remove background noise, the process of translating these readings into position and orientation of the transmitter is begun. We call this process as signal processing and the inverse solution. The algorithm and procedures used to perform it comprise the backward model.

The equation(4-1) predicts the voltage in antenna j caused by the presence of transmitter i as a function of the position and orientation of i as:

$$V_{ij} = g_{ij}(x, y, z, \alpha, \beta, \gamma) \tag{4-1}$$

In the exact form, that should be:

$$V = -N\omega(\overline{A} \cdot \overline{B}) \tag{4-2}$$

$$V = -N\omega(A_x B_x \cos\alpha + A_y B_y \cos\beta + A_z B_z \cos\gamma) \tag{4-3}$$

$$\overline{B} = \sum_{k=1}^{4}\left[\left(\frac{\mu I_i}{4\pi R_k}\right)(\cos\varphi_{k1} - \cos\varphi_{k2})\right]\hat{\theta}_k \qquad (4\text{-}4)$$

where, R, φ, and $\hat{\theta}$ are functions of x, y, z, α, β, and γ ,and the geometry of the receiver. (see, Dave(1995)).

R_k, φ_k, and $\hat{\theta}_k$ are the parameters that describe the relative position and orientation of the transmitter with respect to the receiving antenna.

x, y, and z are positive coordinate of the transmitter in the antenna coordinate system.

α, β, and γ are the direction cosines of the transmitter axis in the antenna coordinate system(see **Figure 4.1**).

V is the voltage induced in the receiver.

V_{ij} is the voltage in antenna j caused by the presence of transmitter i .

$\overline{B}$ is the resultant magnetic flux density. $\overline{B} = B_x\hat{i} + B_y\hat{j} + B_z\hat{k}$.

N is the coil turns of antenna. (N=1 in our experiment).

ω is 2π times the frequency of oscillation.

A is the area vector of the transmitter.

μ is the permeability of the transmission medium, (air)

I_i is the current in the transmitter i (i =1,2,3).

Given x, y, z, α, β , and γ , it is possible to predict V_{ij} by simple substitution. However, the reverse does not true because it is not simple to invert the magnetic flux equation(4-4).

In the inverse solution, given V_{ij}, we seek to determine x, y, z, α, β, and γ, with the help of some mathematical tools such as optimization, initial approximation, perturbation and so on to solve this multiple solution problem. The details can be found in Volcy[Volcy(1994)].

4.6 Model Tests

The objective of the model tests is to demonstrate the accuracy of the tracking system and the real-time data acquisition capability of the tracking system.

Through many preliminary slow data acquisition model tests, we finally chose the free fall test as the main model test for inclined chute flow because both of them are gravitational motion. However, the inclined chute flow has the horizontal flow angle varied from 0 to 25 degrees with static and kinetic friction between chute and spheres while free fall is perpendicular to ground, that is 90 degrees horizontal flow angle without friction between solids. Their motions are analogous in gravitational motion although the flow angle and friction are different.

The concept of the free fall test. The transmitters are implanted in a tracking particle typical of those in the flow mass the same as in chute flow, see **4.2**. The receiving loop antennae are mounted all along the flow area. The signals from the antennae are used to determine the position and orientation of the transmitting tracer particle in a free flow.

The experimental set up is shown in **Figure 4.9.**

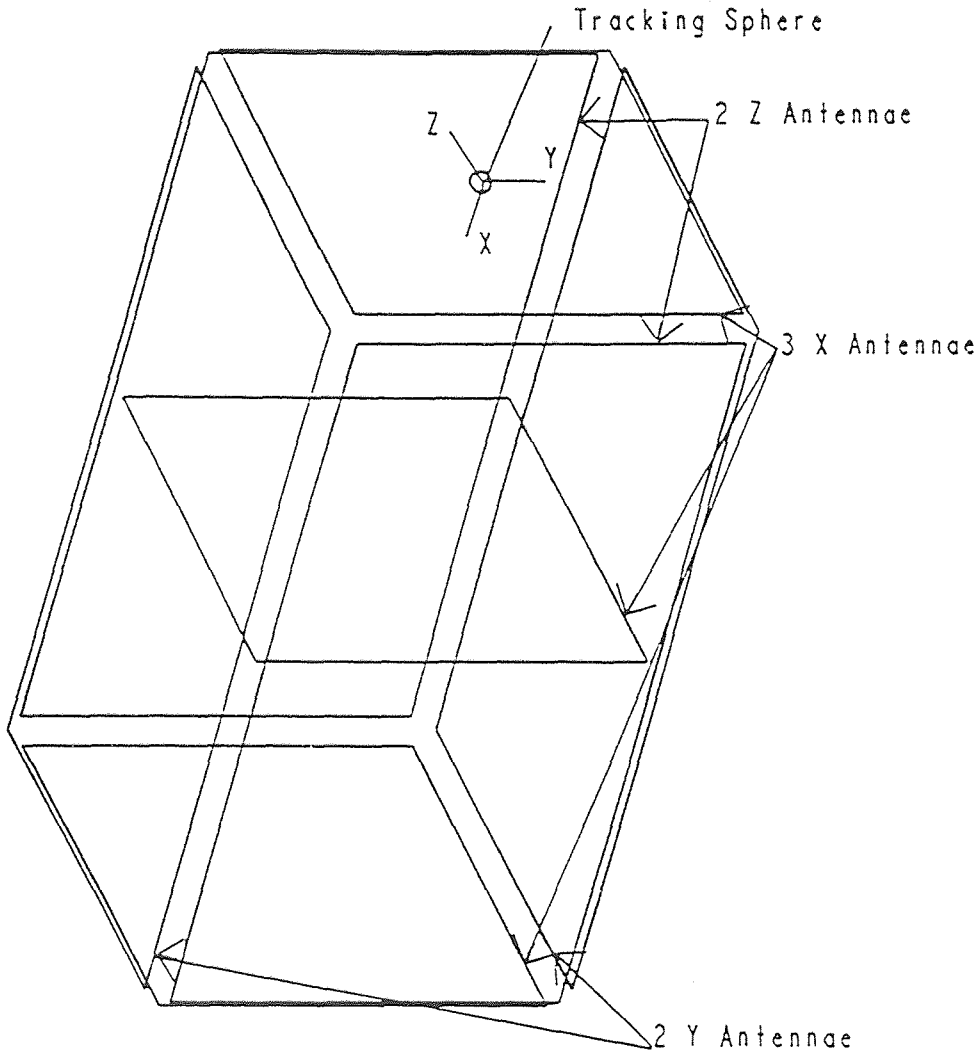

Figure 4.9 The Setup for Free Fall Experiment

The main result of the tests is Shown in **Figure 4.10**[Gupta(1995)]. It is inspiring because the tested gravitational acceleration(383.97 $inch / s^2$ is so closed to the actual gravitational acceleration(386.40 $inch / s^2$) that the relative error is only 0.63%.

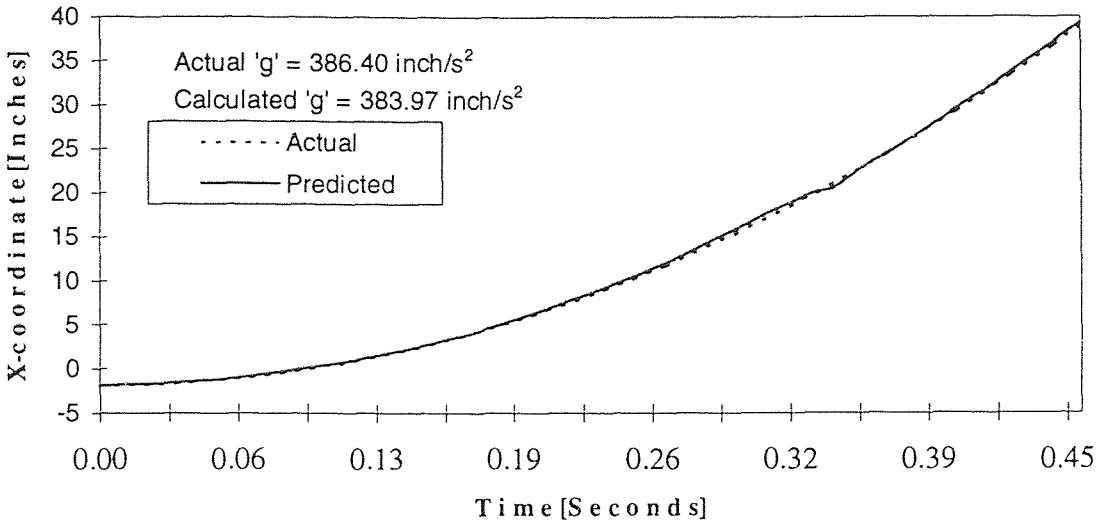

Figure 4.10 The Accuracy of the Tracking System with Gravitational Constant

The maximum error in X is 0.441 inches, in Y is 0.58 inches, and in Z is 0.48 inches. The errors are similar to those obtained with the slow data acquisition rate. The mean errors in X, Y, and Z are 0.11 inches, 0.15 inches, and 0.10 inches respectively. These are slightly better than those obtained with the slow data acquisition rate.

On the whole, both preliminary slow data acquisition model test and free fall test lay a good foundation for the tracking technique to be used in chute flow.

CHAPTER 5

EXPERIMENT PROCEDURES, RESULTS AND ANALYSIS

5.1 Experiment Procedures

The procedures of our experiment are based on the setup that was introduced in **CHAPTER 3**. The sphere flow procedure starts with approximately 60,000 one-inch diameter polyethylene spheres flowing down from the hopper through its adjustable gate. The spheres run out of the entrance box, down the chute through the entrance sluice gate, and finally reach the exit box that is continuously scaled. The vacuum conveyor system is made to return the spheres back to the hopper after the entire mass of sphere have been depleted.

In the flow, there are five factors that can be changed and modulated by the operator:

1. The size of the hopper gate opening (This size varies from 0" to 11.7" and consequently the opening area varies from 0"x0" to 17"x17").

2. The sluice gate opening (It can vary from 0" to 9" height).

3. The chute width (It can be changed from 5" to 14.5" inches).

4. The boundary condition of the chute itself [Both the floor and the walls of the chute can be changed from smooth material (acrylic) to bumpy material (clear prismatic sheet)].

5. The chute inclination angle (It can vary from 0 to 25 degrees).

For experimental calibration, there are three basic methods. They are (1) the scale measurement and data acquisition, (2) the high speed camera, and (3) the tracking sphere technique. These shall be discussed and their results in the following section.

5.2 Scale and Data Acquisition System

The scale system apparatus was introduced in section **3.4**. Our preliminary experiments were carried out on the chute with smooth boundary conditions with a 9" high sluice (chute entrance gate) and a 14.5" chute width. At a rate of five to seven times per second, the scale data acquisition system captured the weight of the spheres while the spheres in the exit box. **Figure 5.1** is a sample of the calibrated results for a 13.7 degrees chute inclination angle.

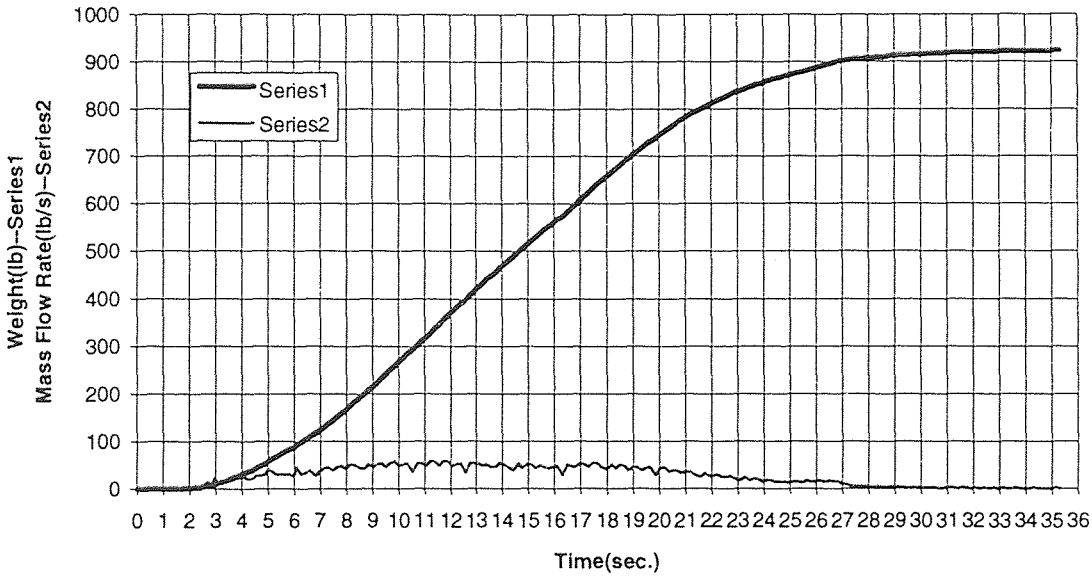

Figure 5.1 Scale Measurement #5 (5/16/1995), 13.7 Degrees, Smooth Floor

In **Figure 5.1**, the curve of Series 1 shows the weight increment (lb.) versus time, while Series 2 show $(\frac{\Delta w}{\Delta t})$ versus time, where Δw is the weight increment in the time interval Δt. For closer observation, the enlarged mass flow rate is shown in **Figure 5.2**.

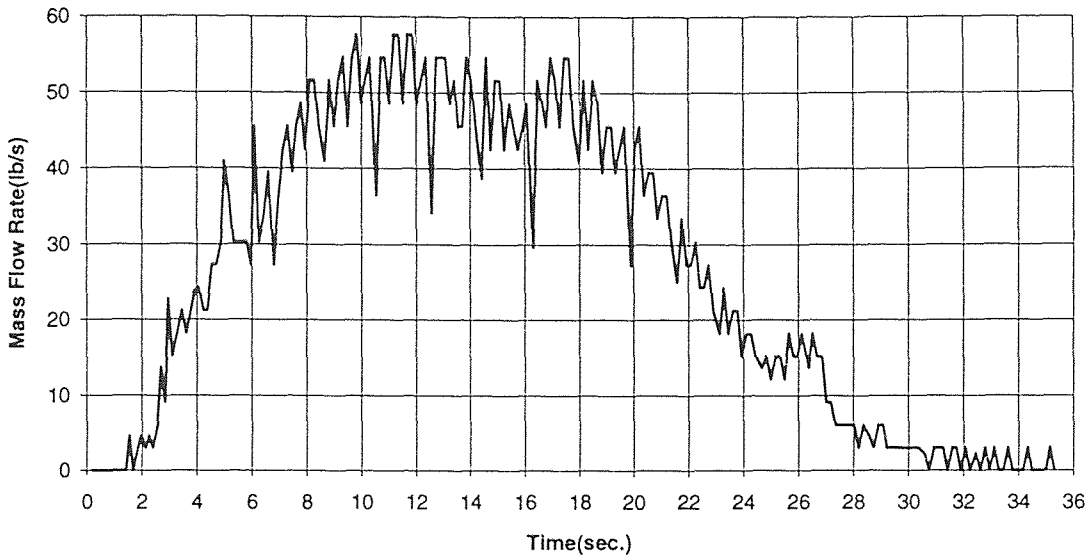

Figure 5.2 Mass Flow Rate #5 (5/16/1995), 13.7 Degrees, Smooth Floor

The results of inclination angles of 8.8 degrees, 10.8 degrees, and 15 degrees with smooth floor and wall conditions are found in the APPENDIX (**Figure A.1 - A.6**, respectively). From these six figures we can know that the maximum mass flow rate of 8.8 degrees, 10.8 degrees, and 15 degrees is found to be 23 lb./s, 46 lb./s, and 70 lb./s respectively as in **Figure 5.3**, Series 1.

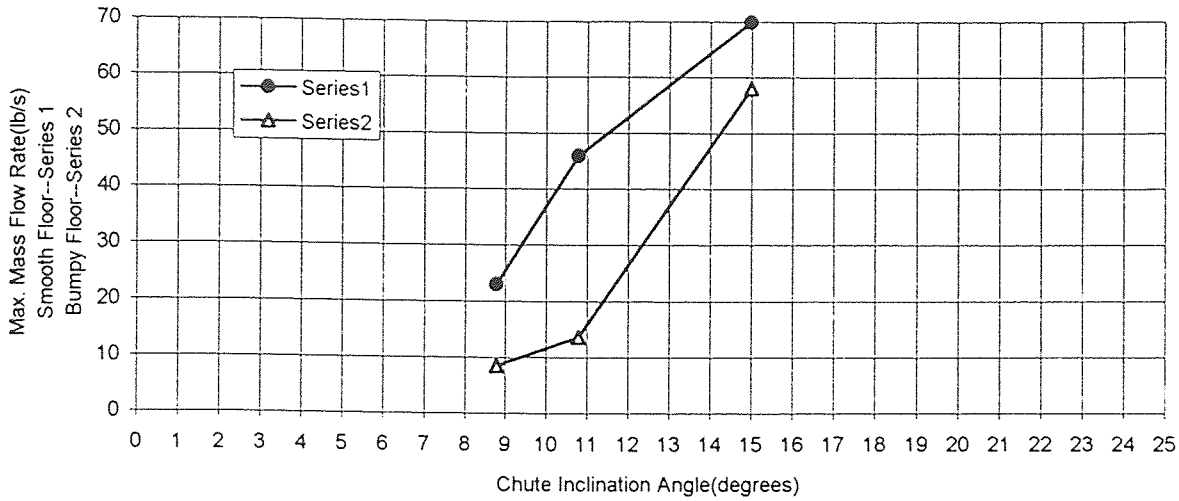

Figure 5.3 The Maximum Mass Flow Rate of Smooth Floor and Bumpy Floor vs. the Chute Inclination Angles

With bumpy floor flow conditions, when the same angles are used as in the previous experiments (i.e. 8.8 degrees, 10.8 degrees, and 15 degrees), results differ as expected (See **Figures A.7 - A.12** in the APPENDIX). The maximum mass flow rates for 8.8 degrees, 10.8 degrees, and 15 degrees are 8.5 lb./s, 13.6 lb./s and 58 lb./s respectively, as shown in **Figure 5.3**, Series2. Upon comparing the two curves in **Figure 5.3**, it is apparent that the mass flow rate increases when the chute inclination angle increases and the smoother the boundary produces a larger mass flow rate.

In order to illustrate the difference in time taken to empty the hopper when the floor is smooth or bumpy for a given inclination, we define a parameter called a Condition Flow Ratio. Thus this ratio is defined as

$$Condition\ Flow\ Ratio = \frac{Time\ to\ empty\ the\ hopper\ when\ floor\ is\ bumpy}{Time\ to\ empty\ the\ hopper\ when\ floor\ is\ smooth} \qquad (5\text{-}1)$$

From both common sense and the experimental results, it is clear that more time is required to empty the hopper when the floor is bumpy than when it is smooth. For instance, the flow in **Figure A.7** (8.8 degrees, bumpy floor) requires 350 seconds for completion, while in **Figure A.1** (8.8 degrees, smooth floor) it took only 130 seconds. This gives a Condition Flow Ratio for 8.8 degrees, 350/130 = 2.7. It is noticed that when the chute inclination angle increases, its Condition Flow Ratio decreases. This principle can also be seen in the bumpy and smooth flow for 10.8 and 15 degrees respectively. From **Figure A.9** (bumpy floor) and **Figure A.3** (smooth floor), the CFR for 10.8 degrees is 155/65 = 2.4, while from **Figure A.11** and **Figure A.5**, CFR for 15 degrees is 40/32 = 1.25. The results are summarized in **Figure 5.4**.

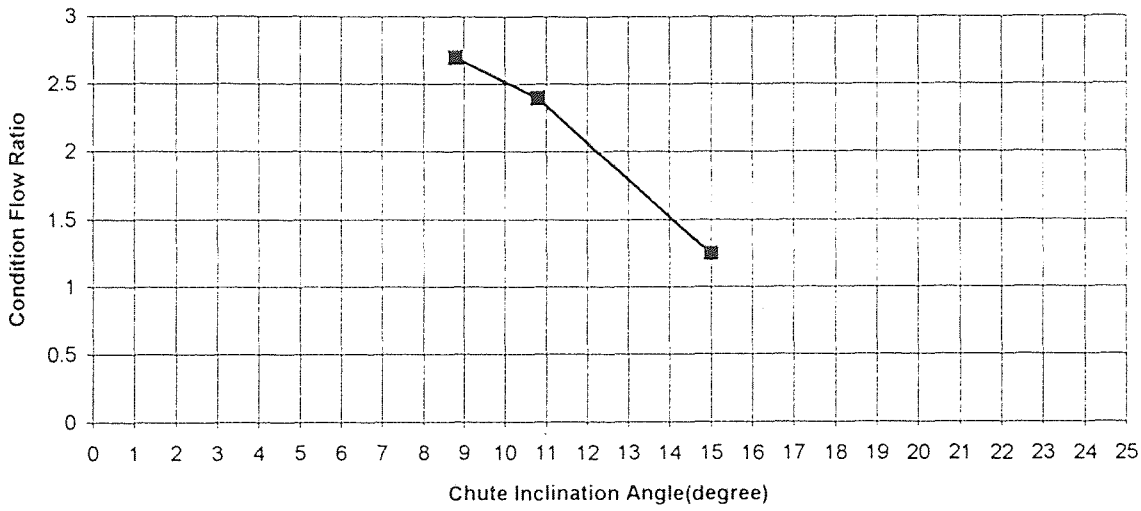

Figure 5.4 Condition Flow Ratio

Hence Condition Flow Ratio shows the influence of chute boundary condition on the flow for chute inclination angles. The greater is the chute inclination angle, the smaller is the influence from chute floor roughness condition.

We note that the spikes in **Figure A.7** and **Figure A.8** were caused by a downward force on the exit box during the flow. The shore flat period of Series 1 in **Figure A.9** and the sudden drop around 80-85 sec was caused by blocking the flow into the exit box. This indicates that the scale is sensitive enough to sense these change.

5.3 High Speed Camera System

The setup of High Speed Camera System is shown up in **Figure 3.8** of **CHAPTER 3**. At a rate of 1,000 frames per second, we let the system's imager is focused on the top layer of flow spheres that are 2 feet from the exit cross section. The time taken by a single sphere to travel through 4" long view of the camera lens (down the chute) is measured, from which its mean velocity can be obtained.

Experiments were carried out of 8.8 degrees, 10.8 degrees, and 15 degrees for both smooth & bumpy chute floors. As the results are from the manually reading of the high speed camera video tapes, and the errors with this kind of reading could not be avoided, the curves of the result are very rough. But, these curves do show some trends. Results are shown in the plots of **Figure A.13 - A.18** in the APPENDIX. **Figure 5.5** summarizes the velocity calculations of **Figure A.13 - A.14** (smooth vs. bumpy floor at an inclination of 8.8 degrees).

The follow observations and conclusions are drawn from these results.

1. The spheres are in the status of free flow at the beginning period of the chute flow, that is no bulk mass is formed here. The spheres are in the status of cohesive flow at the normal bulk flow period. The cohesive flow means that the spheres heap up in the sticklike status in the flow.

2. The velocity of free flow is faster than the velocity of cohesive flow. From **Figure 5.5** we can see that this pattern is followed for both the smooth and bumpy floors.

3. The spheres in smooth floor flow are more cohesive than in bumpy floor flow which will be explained by the results in section **5.4**.

4. With the same chute inclination angle, the sphere velocity in smooth floor condition is obviously faster than in bumpy floor condition.

5. Under the same boundary conditions, the larger the chute inclination angle, the faster the velocity of the flowing sphere.

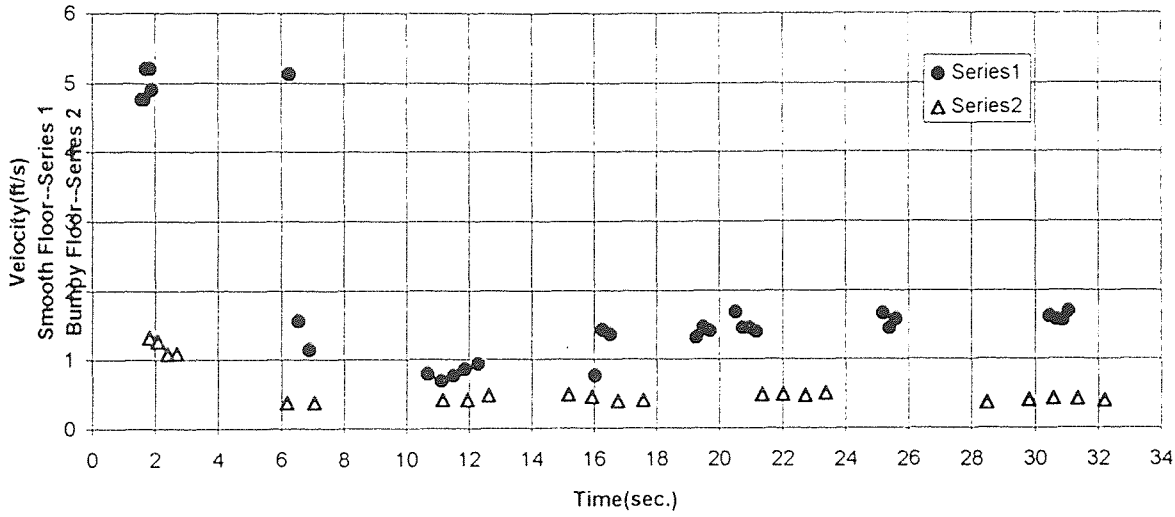

Figure 5.5 High Speed Camera Results of Smooth and Bumpy Floor, 8.8 Degrees

5.4 Distribution of Flow Layers

The distributions of sphere layers in the flow were measured in the 8.8 degrees of chute inclination condition. This kind of measurement was carried out by measure the sphere flow depth through reading four rulers that were glued on the wall of the chute. The results are shown in **Figure 5.6**. As this kind of measurement is in the rough naked eye observation stage, the result is for reference only. But, a trend showing a decreasing depth along the chute was observed. This means that the bulk or mean flow velocity is increasing. The fundamental theory tells us that the velocity is tending to reach a maximum or "terminal" value if the chute is long enough [Woodcock(1987)]. That is to say the maximum velocity will not be reached until the flow depth remains unchanged along the length of the chute.

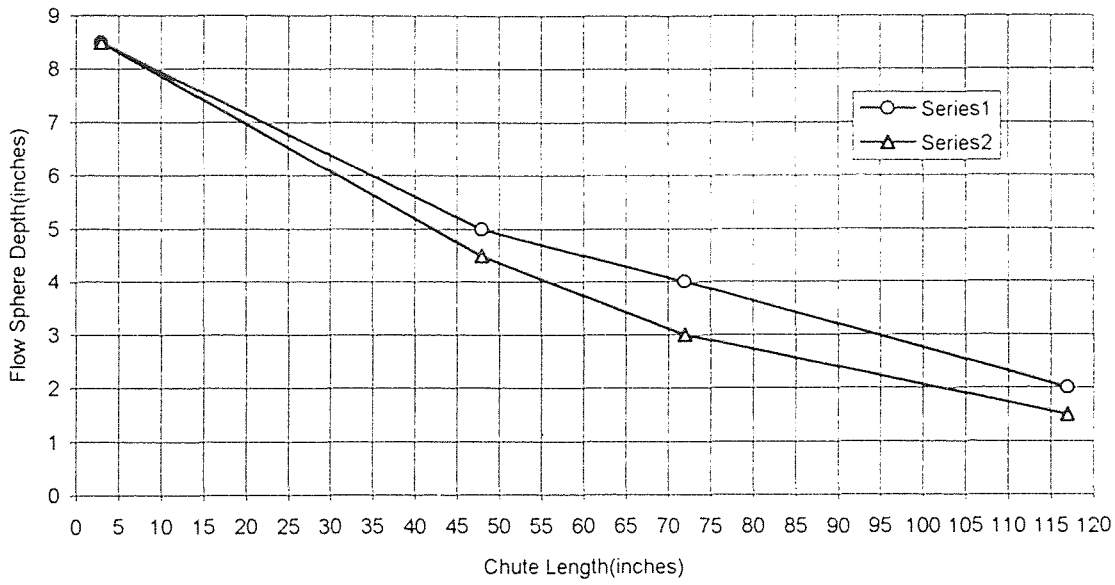

Figure 5.6 Distribution of Flow Sphere Layers
in 8.8 Degrees of Chute Inclination

5.5 Tracking Sphere System

This latest calibration technique's research in our experiment is a difficult work and it needs long term effort. Although it works well at the linear measurement in free fall model test, the system still faces challenge in its application on chute. As of now, the status is: the linear mean error of the measurement has been as good as 0.2 inches to 0.3 inches. The angular mean error of the measurement is 10 degrees and the results are not stable. It takes time to figure out the problem in measurement and it needs continuous research. The results of this technique will be compared to the results of high speed camera after this experiment is completed. The experiment procedures and details are shown in Dave(1995) and Volcy(1994).

CHAPTER 6

SUMMARY AND FUTURE WORK

6.1 Summary of Progress

A chute flow experimental setup has been built, The chute flow experiments have begun and three types of tests have been used in the experiments.

Building the experiment apparatus required several individual components: A huge supply hopper on a tall framework was erected after careful consideration of its slope-sheet angle and careful stress calculations of the support structure. A flexible antenna system composed of 27 loop antennae was mounted on the chute. One of the most challenging problems was the conveyor system. To avoid influencing the electro-magnetic field that the tracking sphere and antenna system rely upon, we could not use a metal conveyor. Through intensive investigation, calculation, and consideration, we realized that no conveyor could recirculate the spheres with adequate flow speed unless made of metal. We had to give up the recirculation idea. Finally we found the vacuum system to be the best choice in a non-recirculating system given the limited space and budget. The entrance box was rebuilt for greater strength. The exit box was designed and built without difficulty. After much arduous work in design, purchase, and fabrication, we are ready for experiments.

In the experiment, about 60,000 spheres were put into flow. Not only was the chute angle changed into 8.8 degrees, 10.8 degrees, 13.7 degrees, and 15 degrees

separately, but also the chute flow floor was changed from smooth to bumpy texture in each individual angle condition. The three main testing means: scale data acquisition system, high speed camera system, and antenna data acquisition system have all been used in experiments. With the scale data acquisition system, we obtain the mass flow rate results for four different chute flow angles and both smooth and bumpy chute floor boundary conditions for each angle. With the high speed camera, we obtain the flow sphere velocity in the surface layer of the flow bulk and found that the large mass flow of the spheres is in the state of cohesive flow. The velocities were observed for the three different chute flow angles of 8.8 degrees, 10.8 degrees, and 15 degrees. For each angle, smooth and bumpy floor boundary conditions were used. The data acquisition system can be used in an actual chute flow although its results require further improvement. The development of the tracking sphere and its data acquisition system is a long term project and will take same time for complete development.

6.2 Direction for Future Work

Much work remains to be done to perfect the chute flow experiments. There are four main directions in which to proceed.

1. The scale (weight) measurement time interval should be constant so that the computer software can smooth the results of the scale data acquisition system. At present, the frequency of the scale calibration has obtained 10 times per second. Although the time intervals still can not exactly match the constant, the faster calibration speed makes them more relatively closer to the constant desired.

2. The antenna data acquisition system, associated with the tracking sphere, should be further used with the actual chute flow. Its results should be used to indicate sphere velocity and be compared with the corresponding velocity found by the high speed camera.

3. More experiments should be conducted to study if there is any possibility for the sphere velocity to reach the terminal value in the chute. That is to find the aspect when there is no decreasing depth in the granular flow layers. There are two ways to look for this phenomenon: one is to decrease the chute inclination angle, the other is to narrow the chute depth.

4. According to the above results, a decision can be made about a chute extension and how long is optimum chute length. The chute extension is a big undertaking and needs our careful thought. A chute extension will result in much effort such as a hopper extension, conveyor capacity enlargement, chute supports change, and so on.

6.3 Conclusions

This inclined chute particulate flow experiment with non-intrusive tracking technique and other modern calibration means has been built and its use has begun. As indicated in the introduction, this project is part of a contract funded by the U. S. Department of Energy. After completion of this research, the chute flow facility will be incorporated into a new laboratory now under development. This facility is part of our NSF-funded curriculum development and will be used for both undergraduate and graduate Particle Technology.

APPENDIX

FIGURES OF CHAPTER 5

Figure A.1 Scale Measurement #12 (7/26/1995), 8.8 Degrees, Smooth Floor

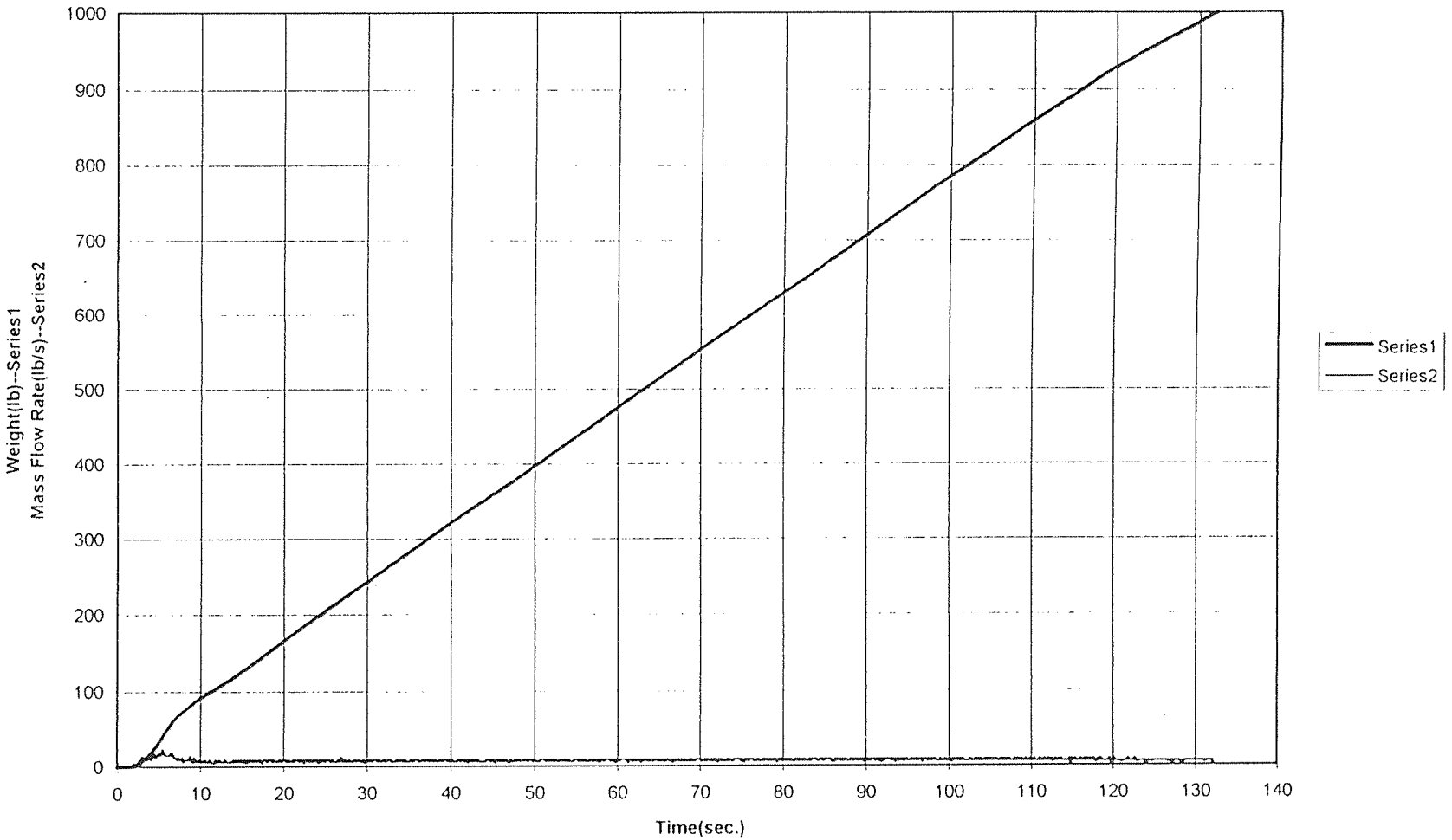

Figure A.2 Mass Flow Rate #12 (7/26/1995), 8.8 Degrees, Smooth Floor

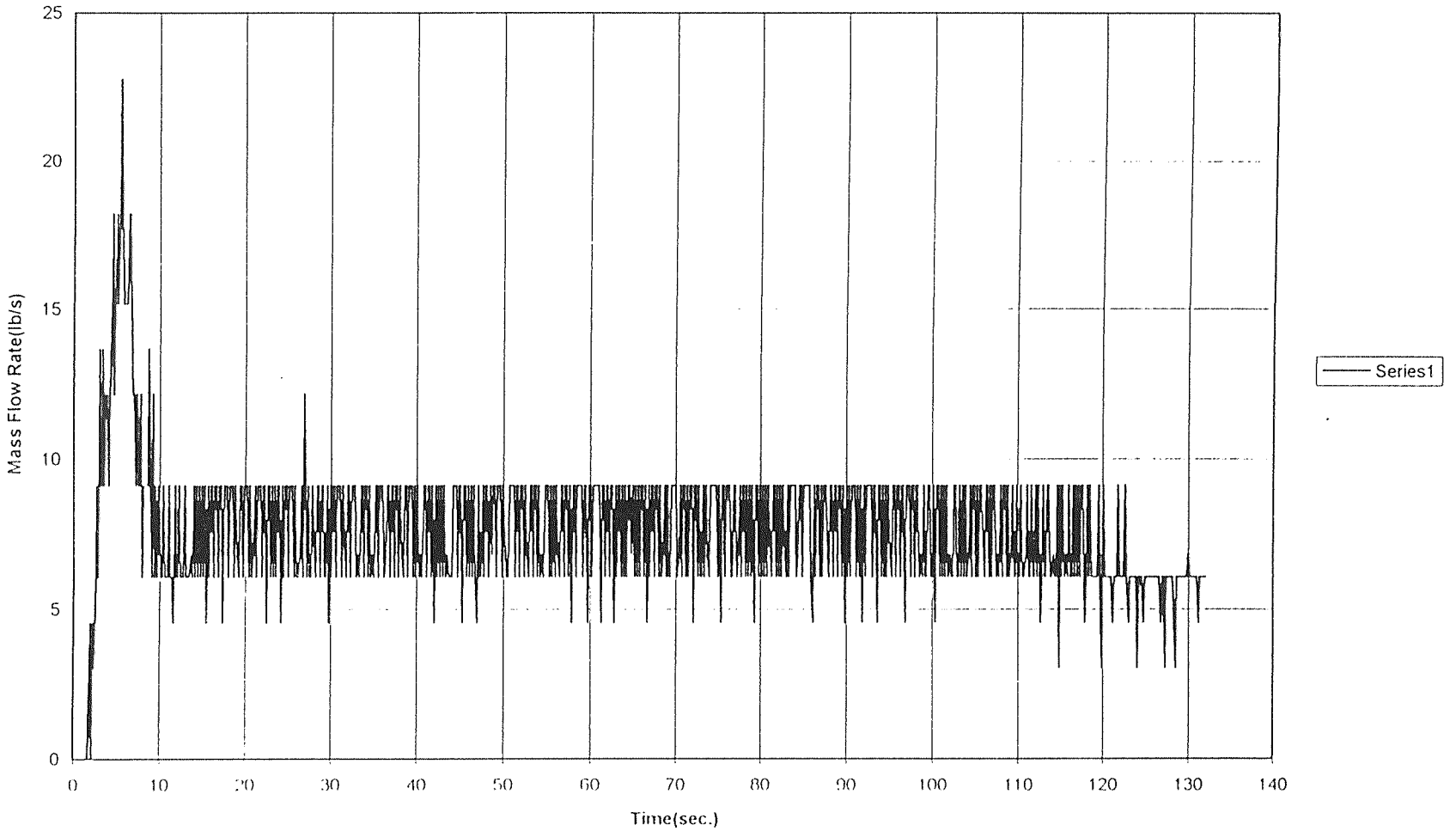

Figure A.3 Scale Measurement #8 (7/18/1995), 10.8 Degrees, Smooth Floor

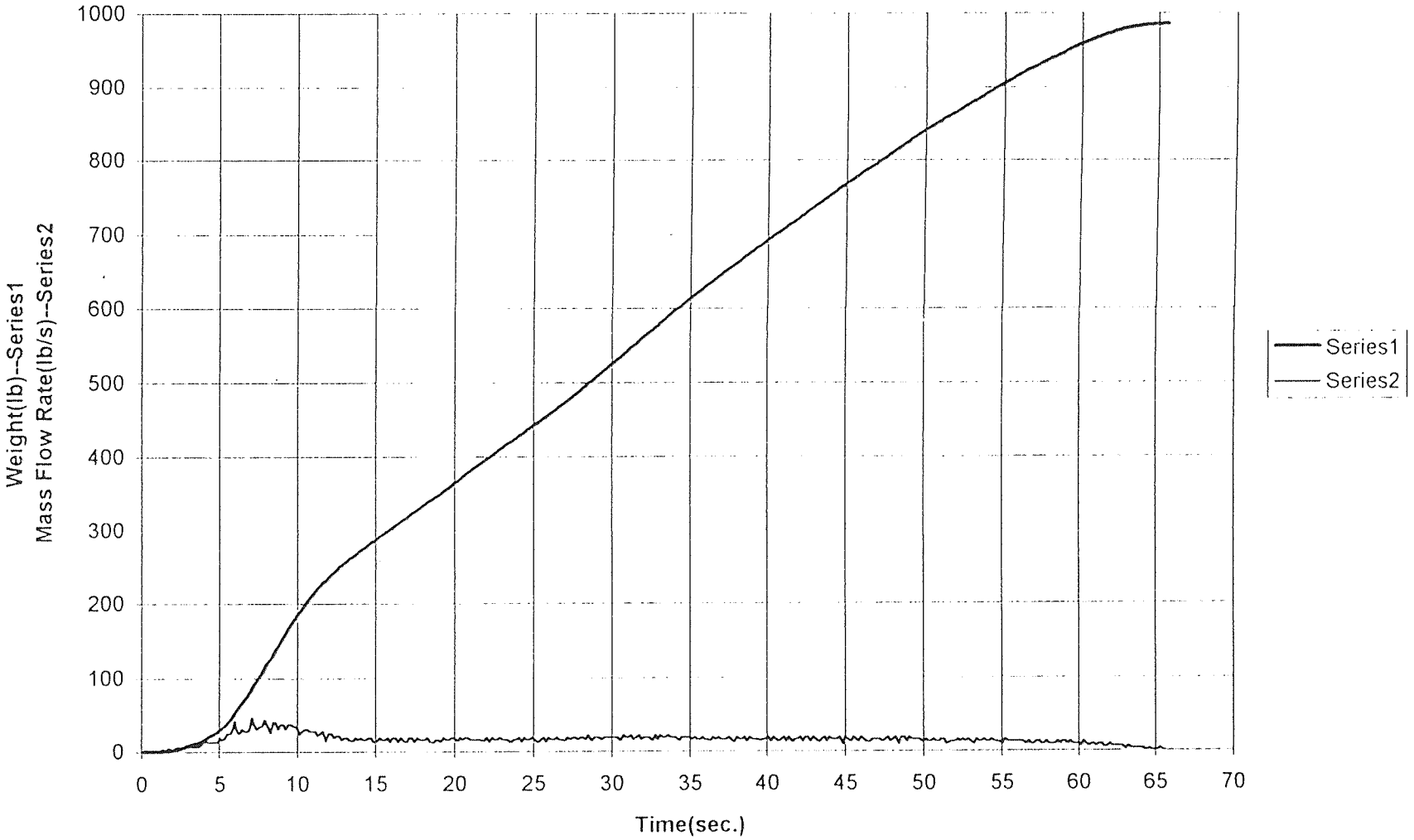

Figure A.4 Mass Flow Rate #8 (7/18/1995), 10.8 Degrees, Smooth Floor

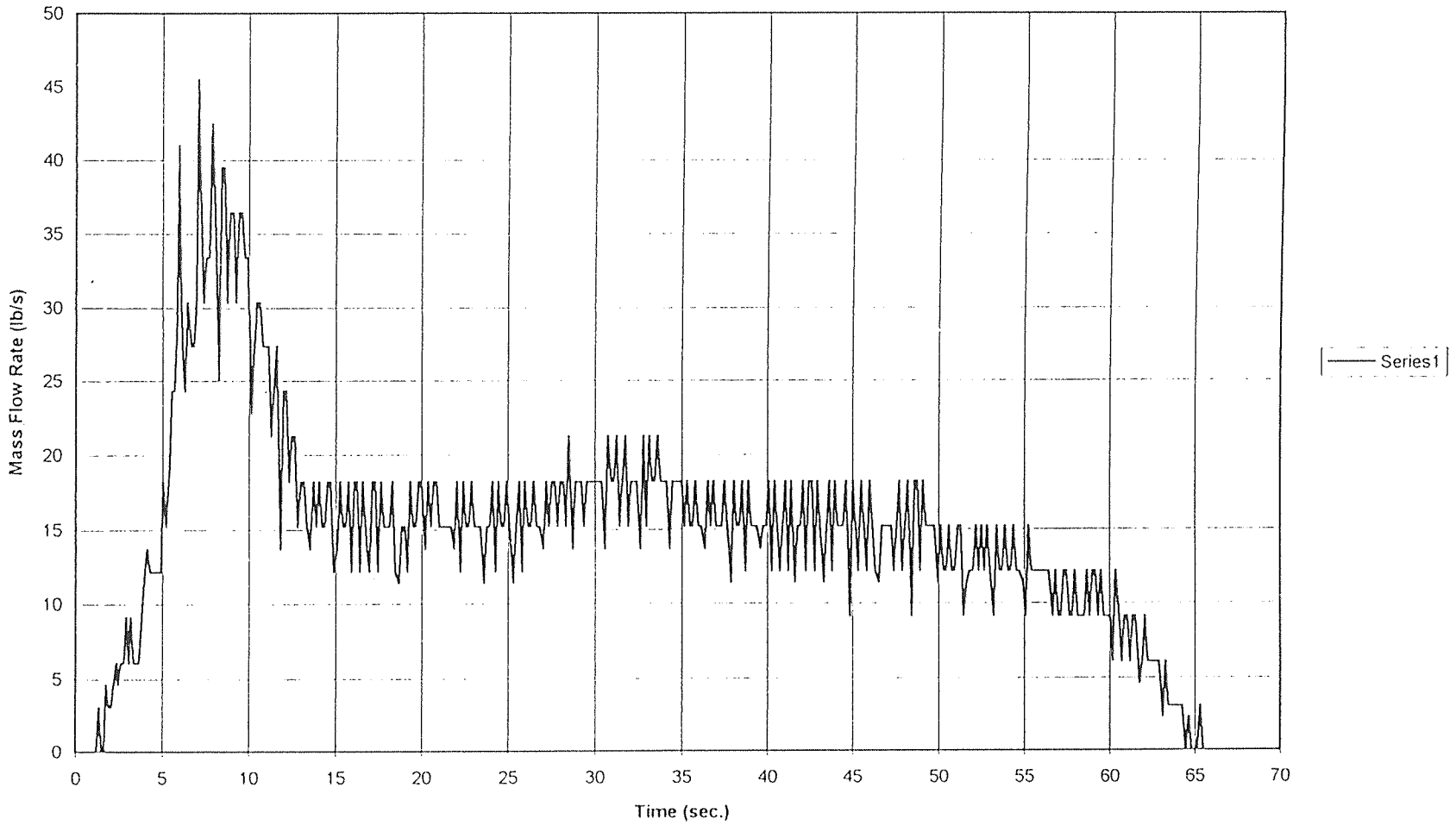

Figure A.5 Scale Measurement #11 (7/25/1995), 15 Degrees, Smooth Floor

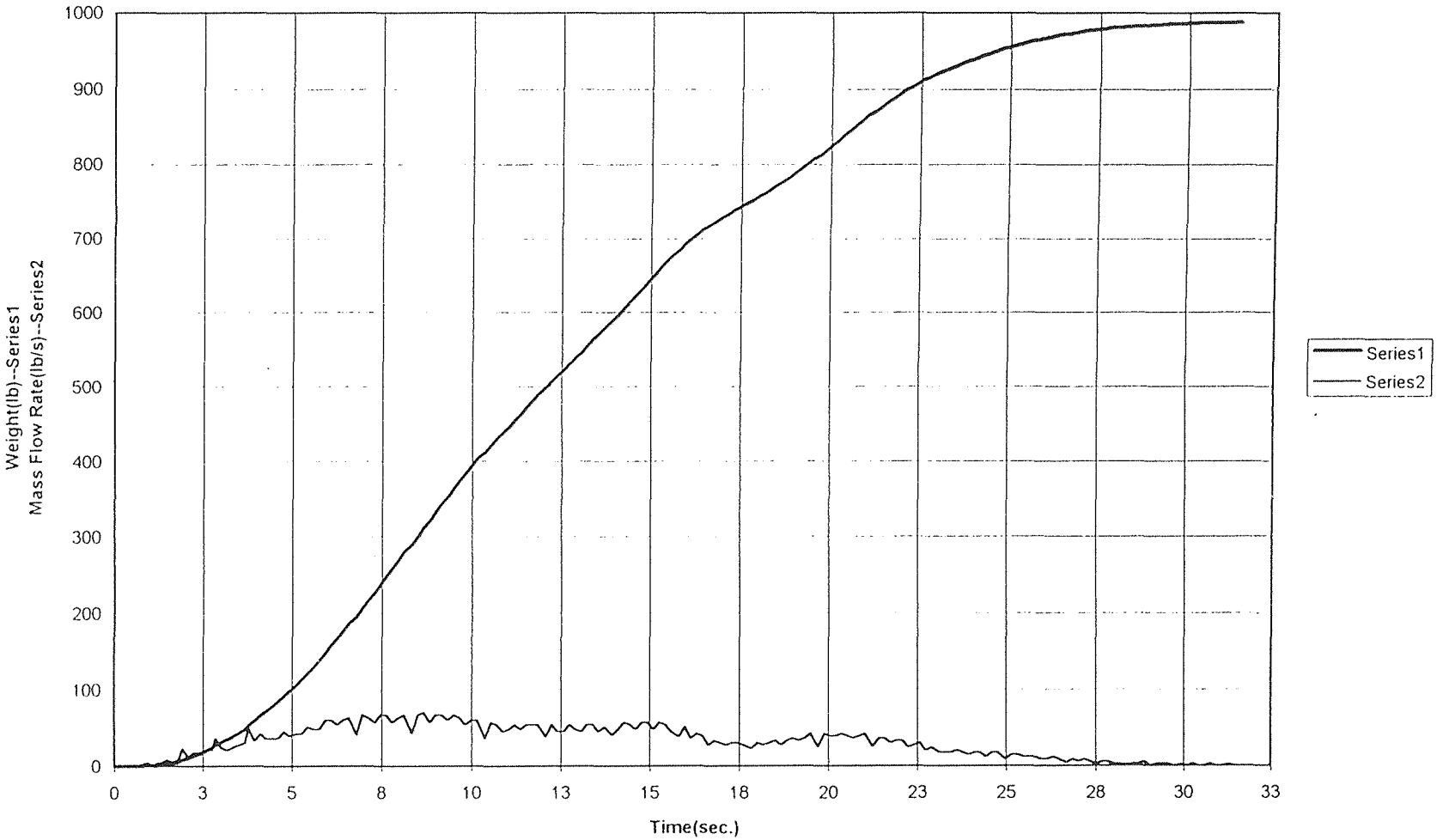

Figure A.6 Mass Flow Rate #11 (7/25/1995), 15 Degrees, Smooth Floor

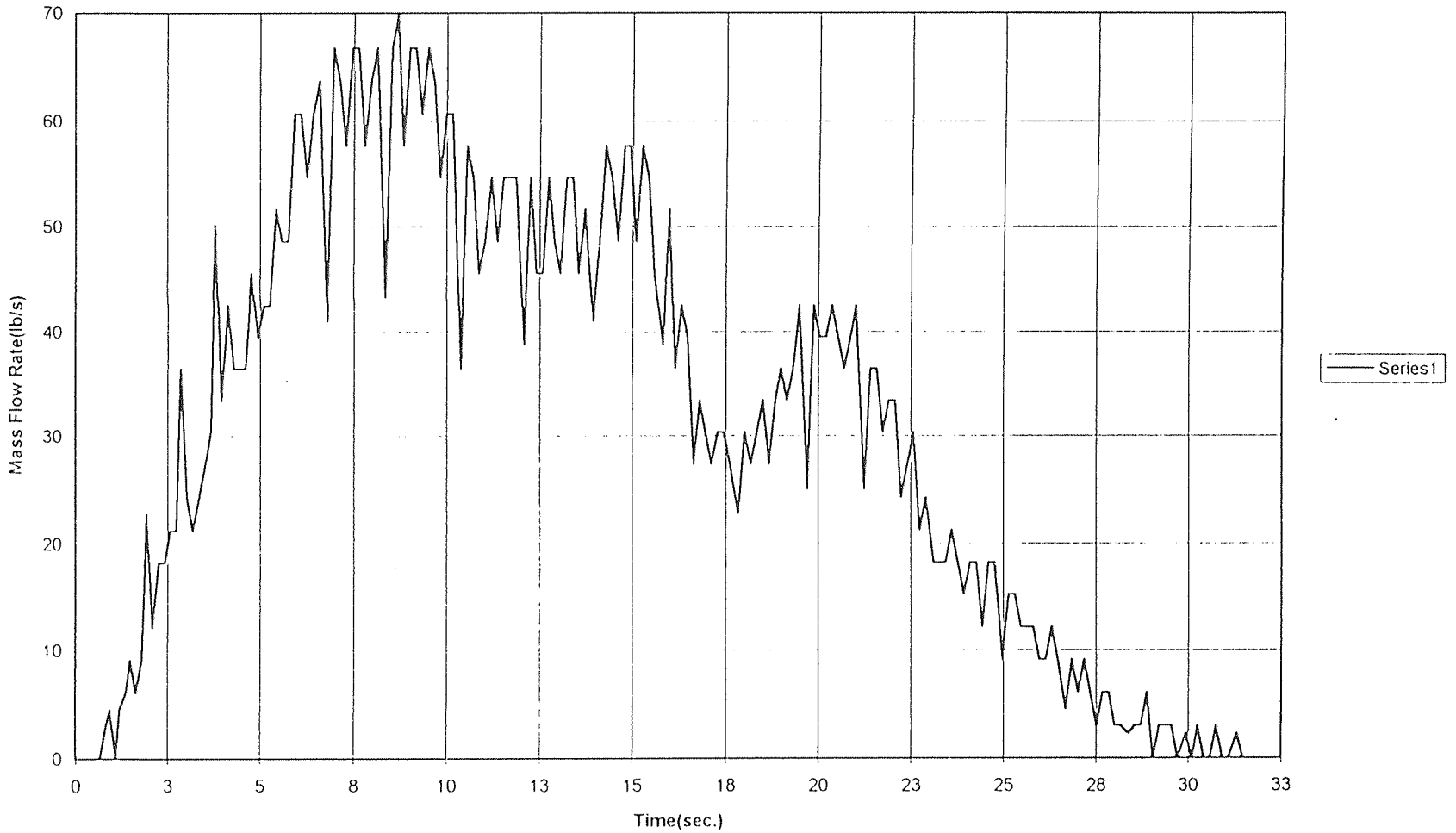

Figure A.7 Scale Measurement #13 (7/27/1995), 8.8 Degrees, Bumpy Floor

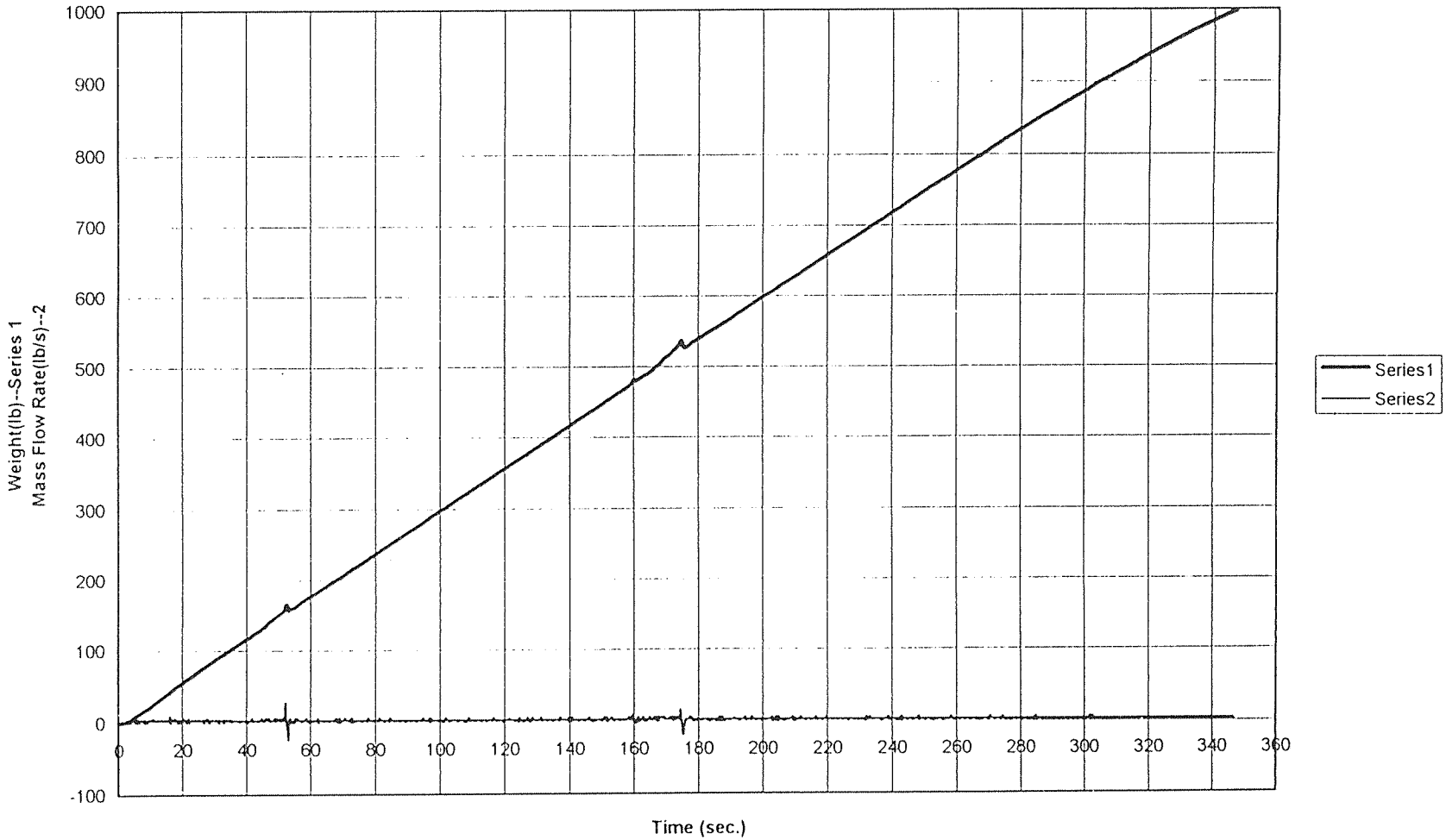

Figure A.8 Mass Flow Rate #13 (7/27/1995), 8.8 Degrees, Bumpy Floor.

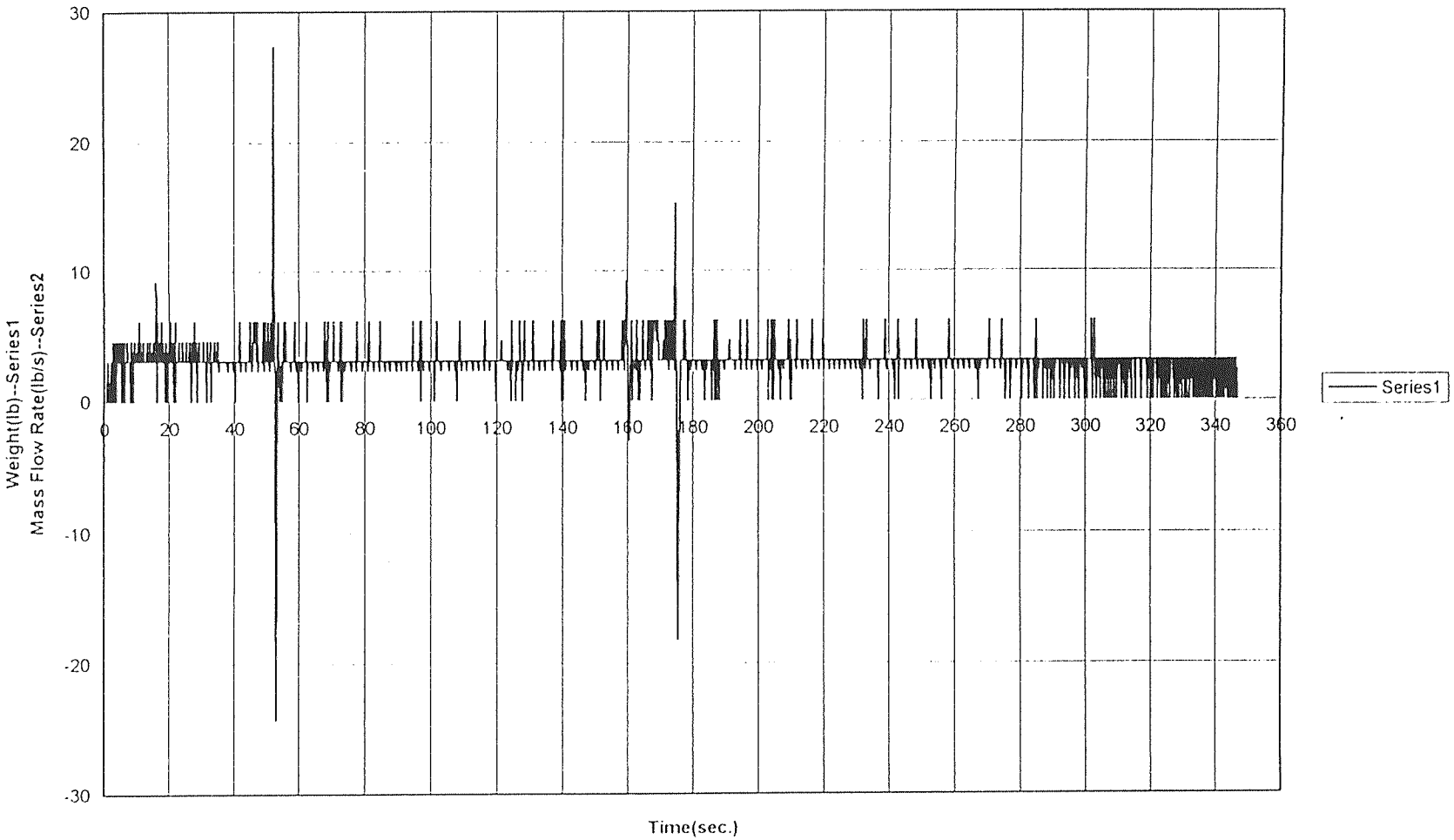

Figure A.9 Scale Measurement #9 (7/21/1995), 10.8 Degrees, Bumpy Floor

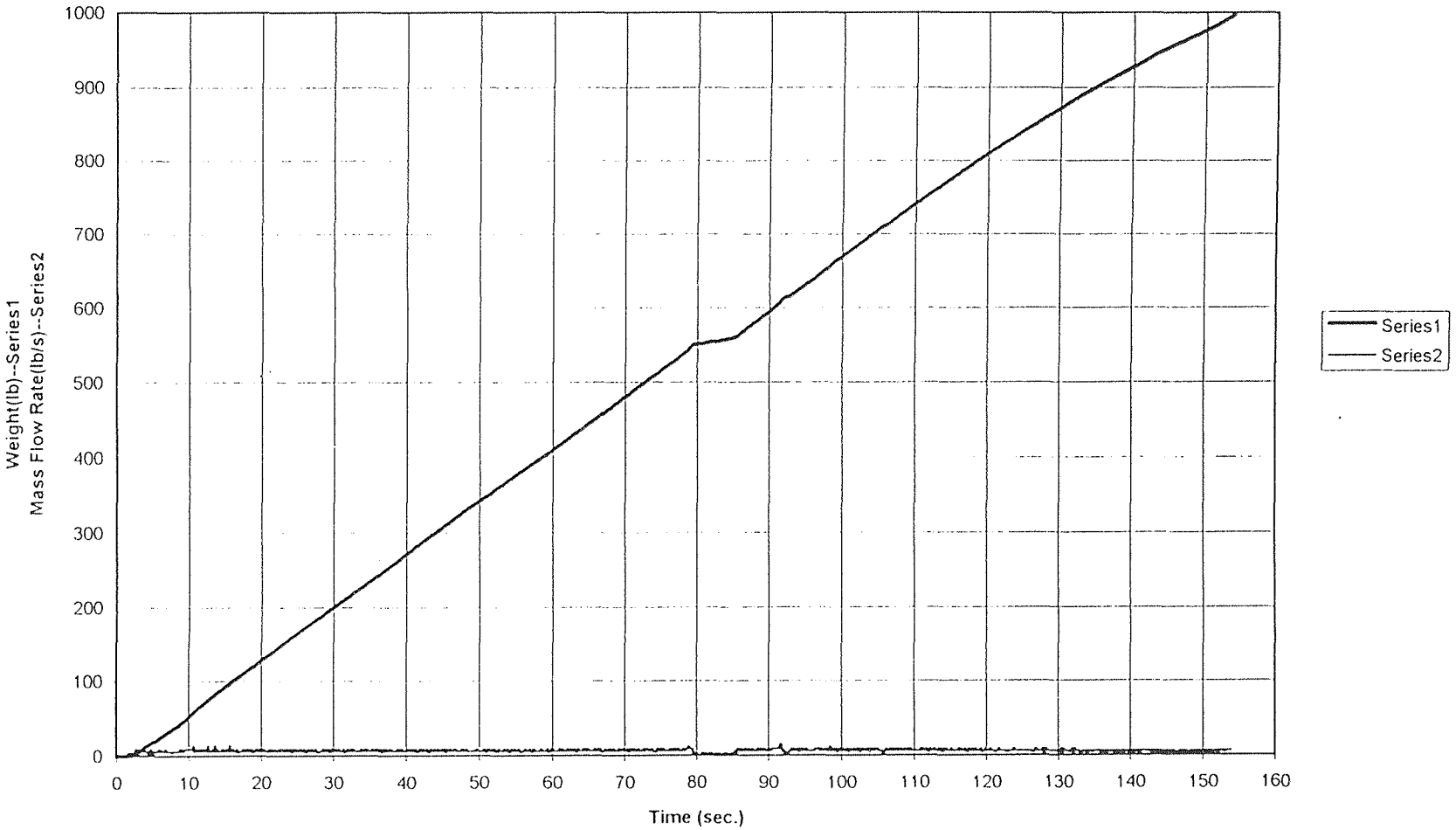

Figure A.10 Mass Flow Rate #9 (7/21/1995), 10.8 Degrees, Bumpy Floor

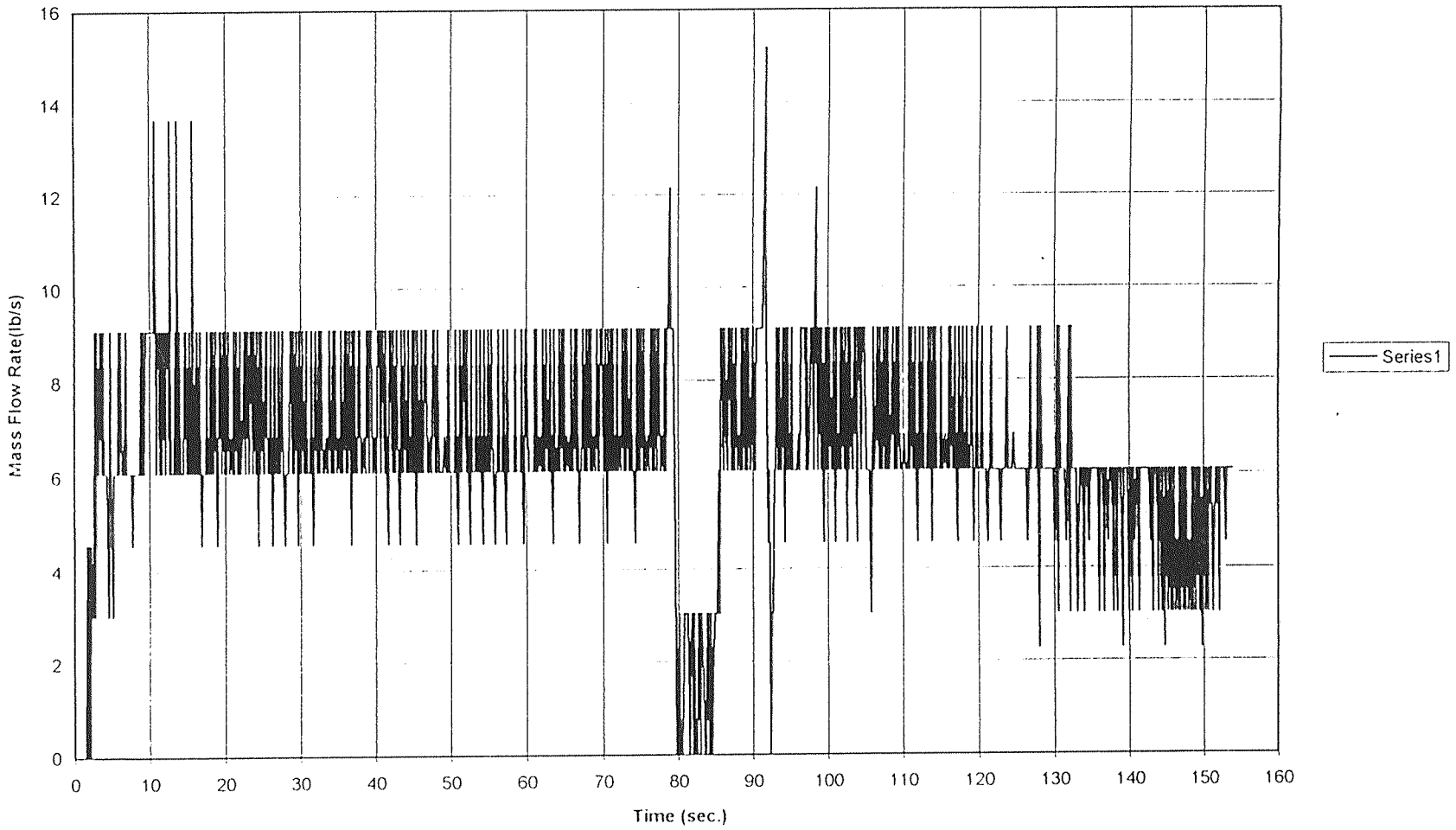

Figure A.11 Scale Measurement #10 (7/25/1995), 15 Degrees, Bumpy Floor.

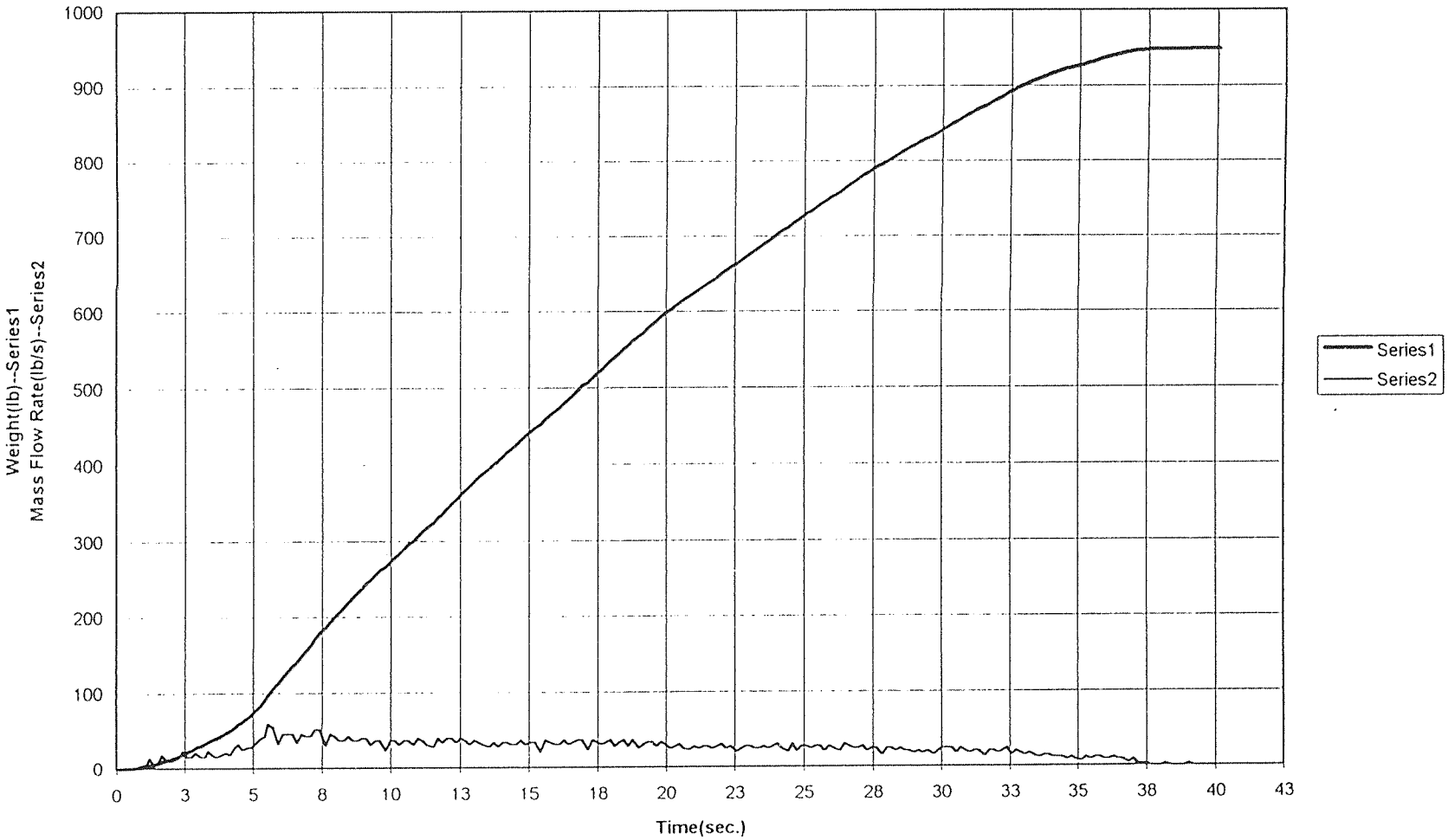

Figure A.12 Mass Flow Rate #10 (7/25/1995), 15 Degrees, Bumpy Floor

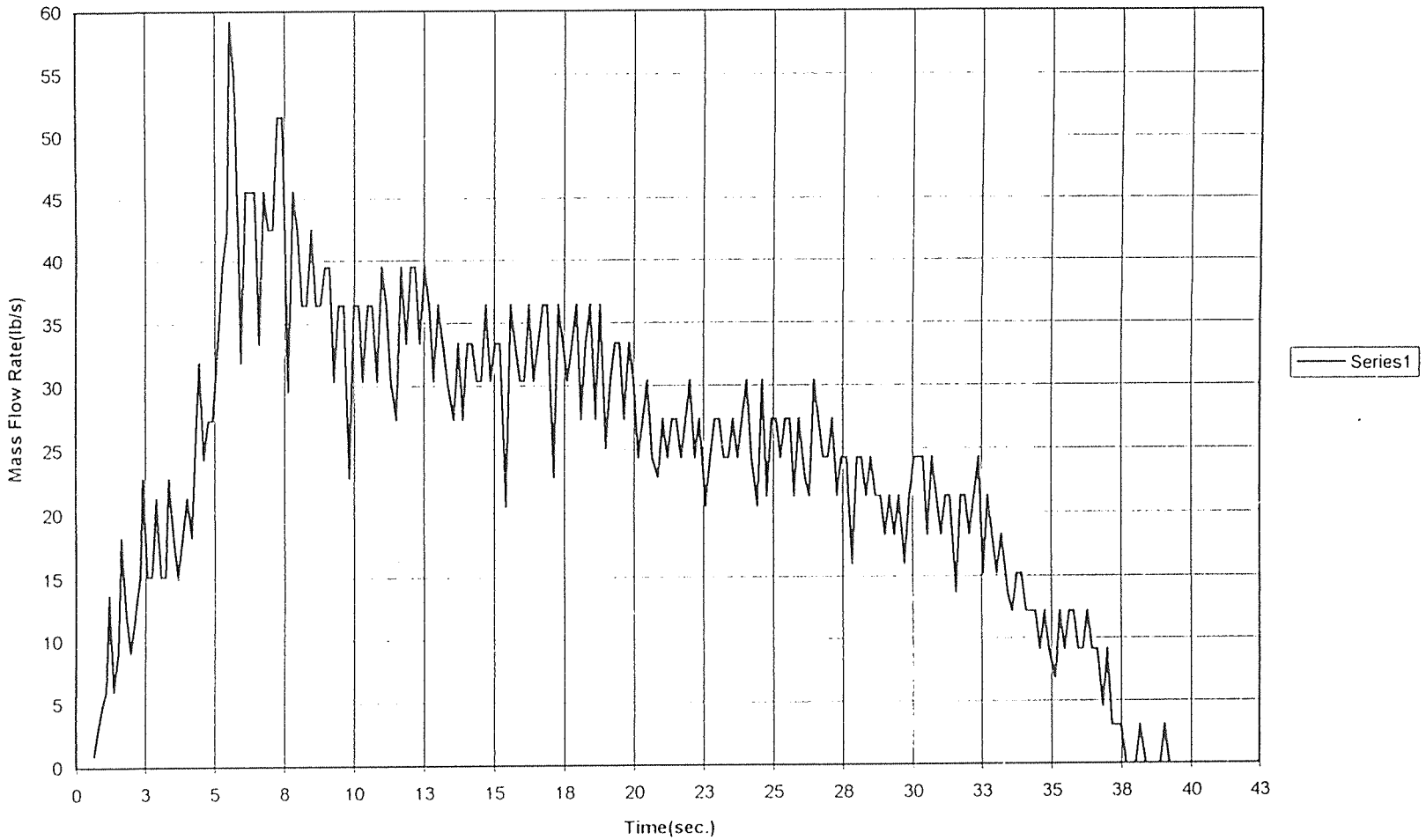

Figure A.13 High Speed Camera Results, 8.8 Degrees, Smooth Floor, 7/26/1995

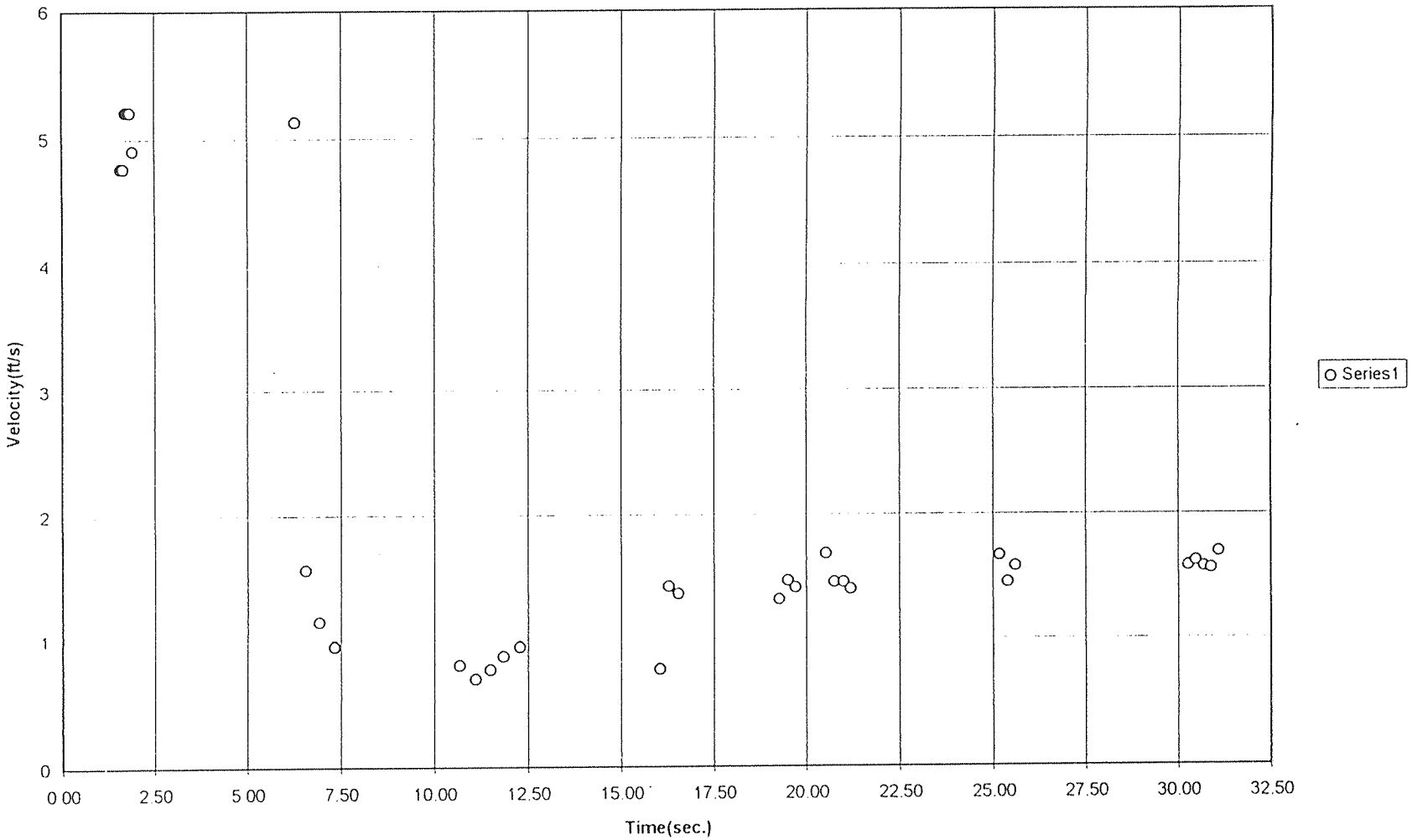

Figure A.14 High Speed Camera Results, 8.8 Degrees, Bumpy Floor, 7/27/1995

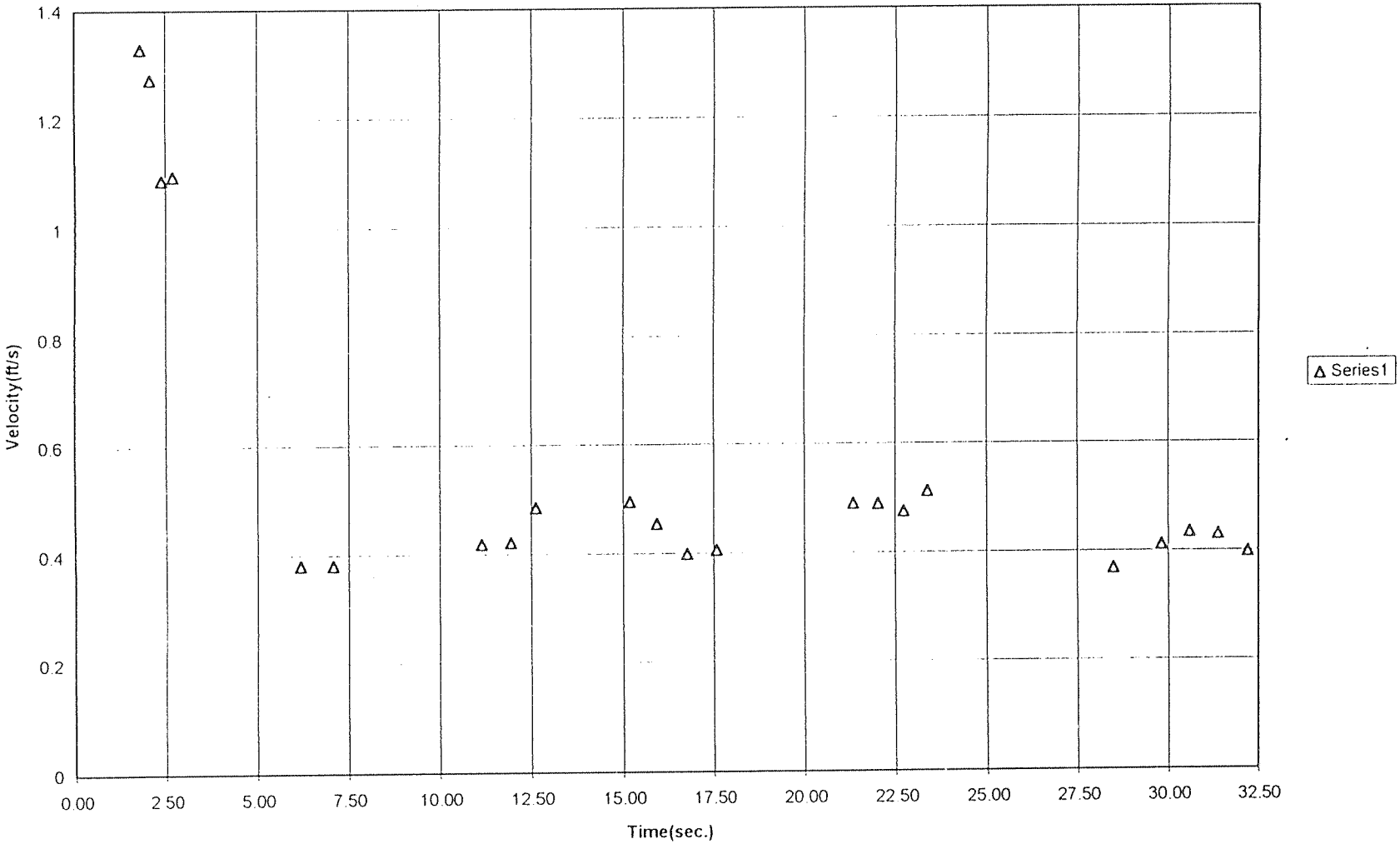

Figure A.15 High Speed Camera Results, 10.8 Degrees, Smooth Floor, 7/18/1995

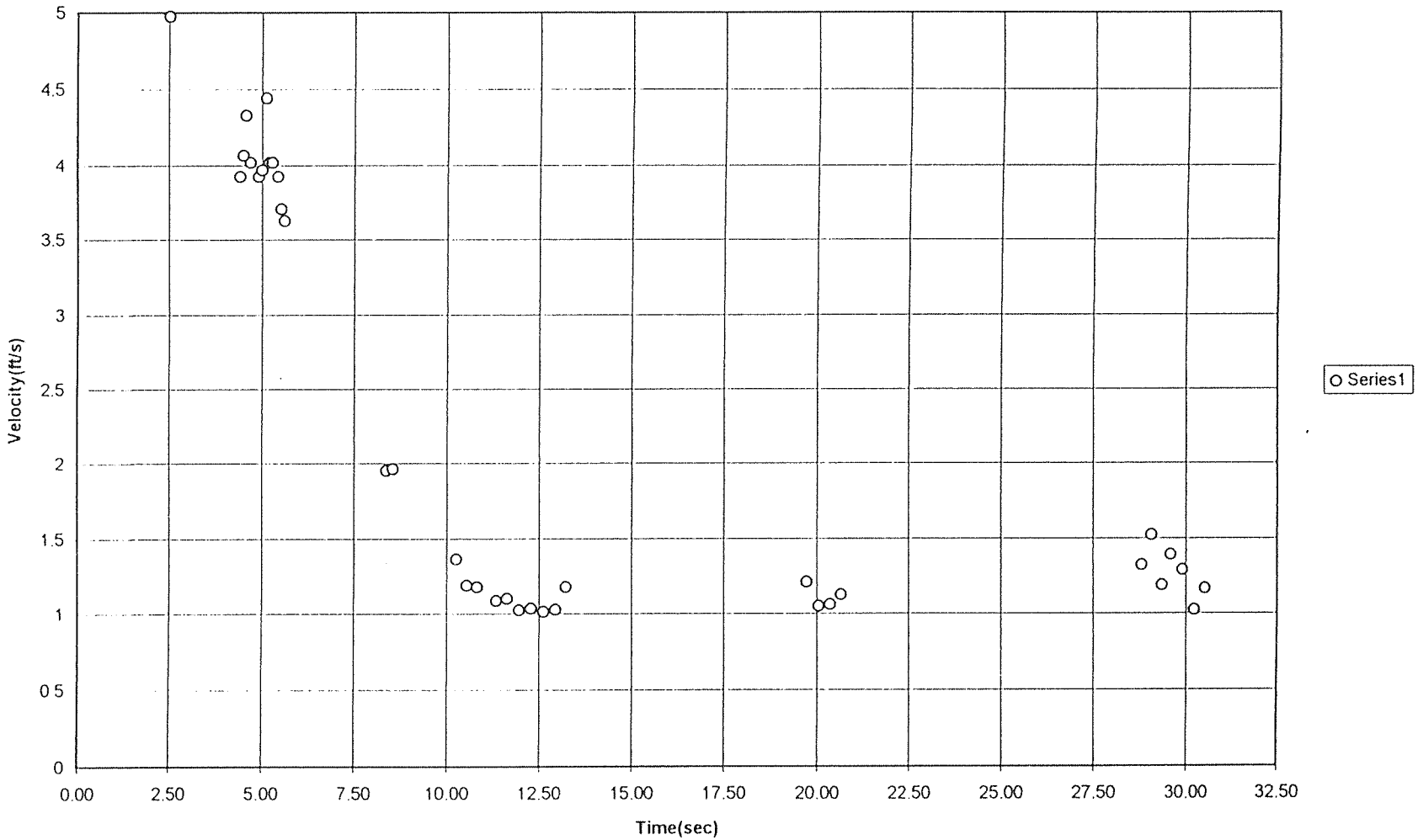

Figure A.16 High Speed Camera Results, 10.8 Degrees, Bumpy Floor, 7/21/1995

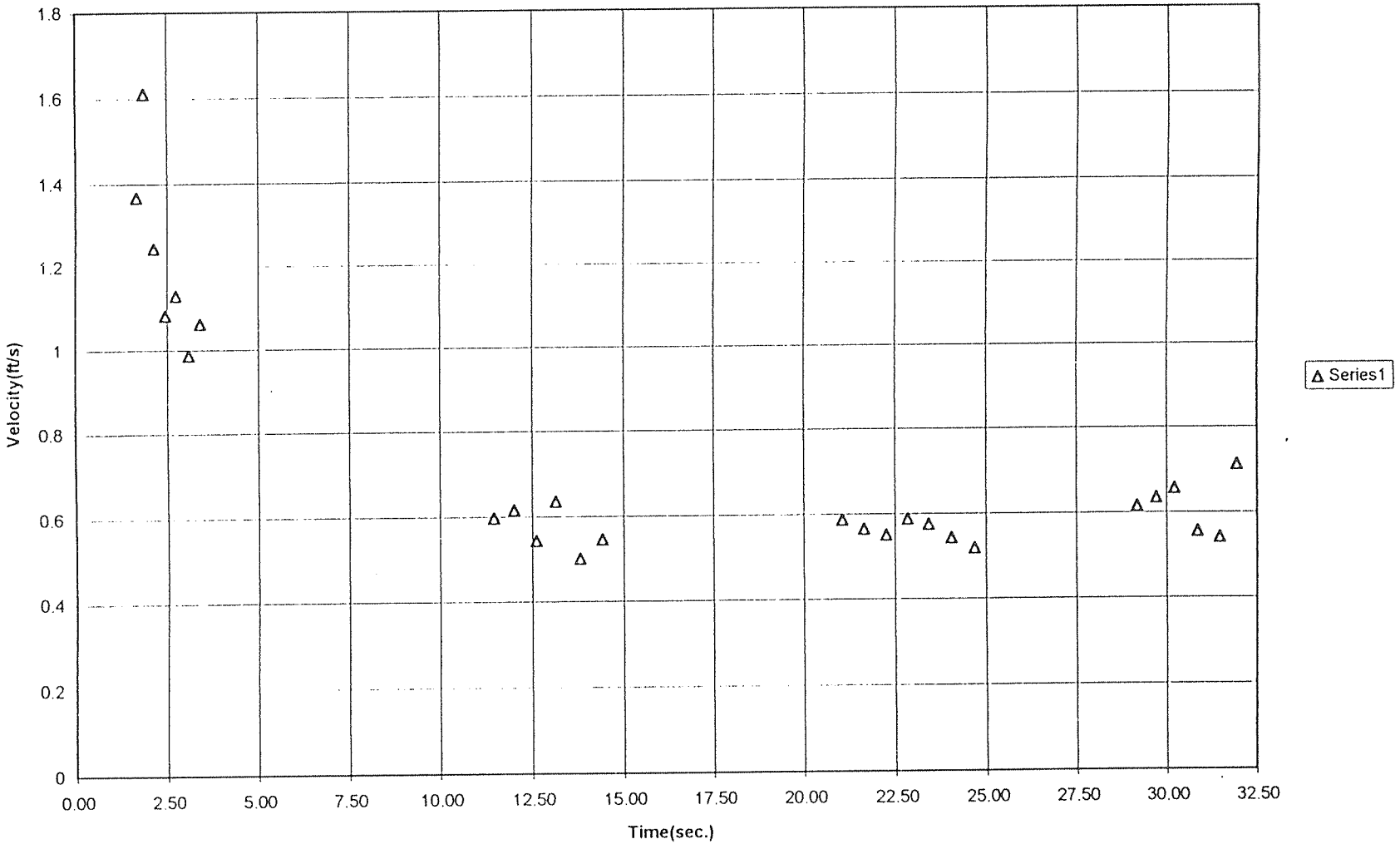

Figure A.17 High Speed Camera Results, 15 Degrees, Smooth Floor, 7/25/1995

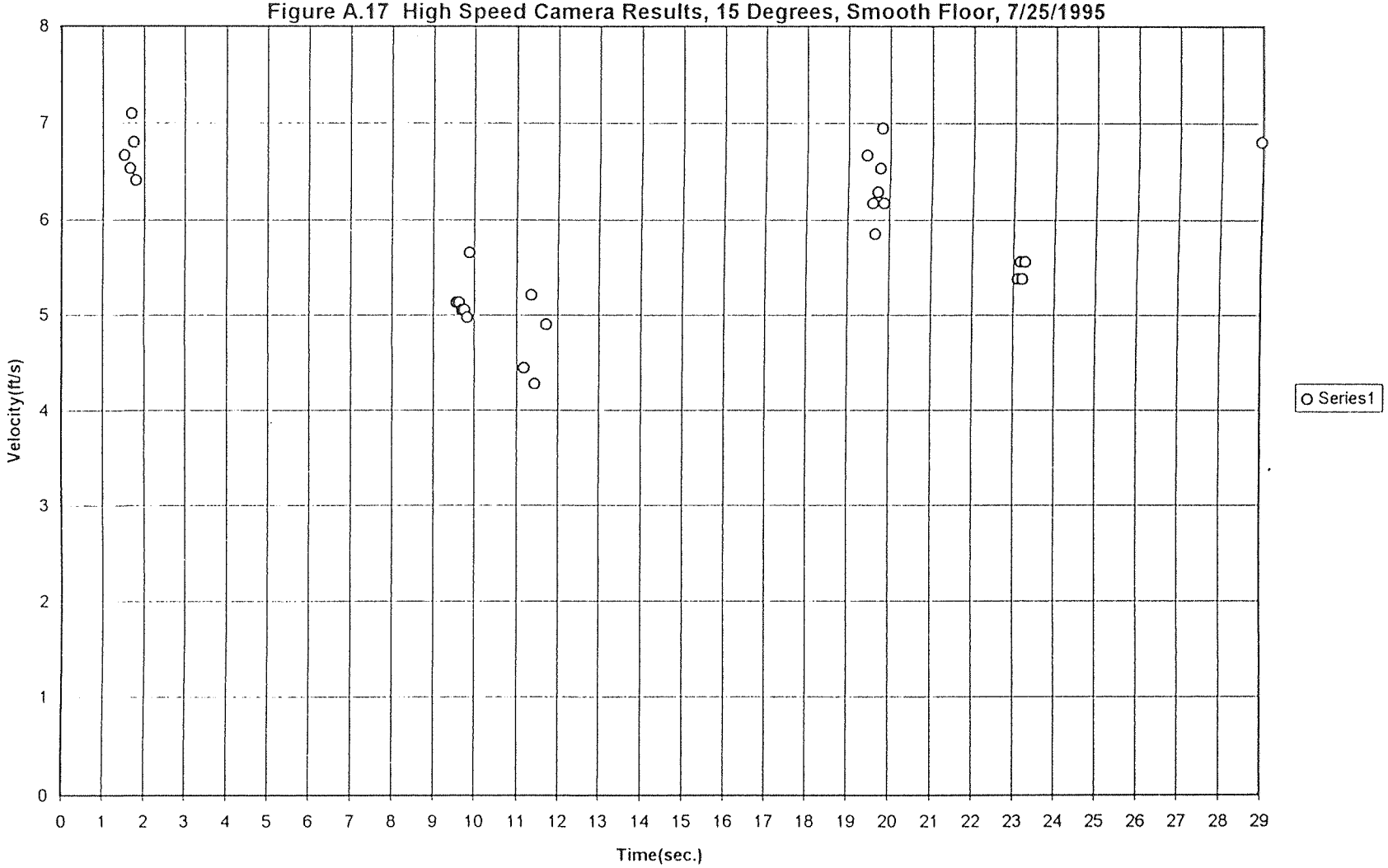

Figure A.18 High Speed Camera Results, 15 Degrees, Bumpy Floor, 7/25/1995

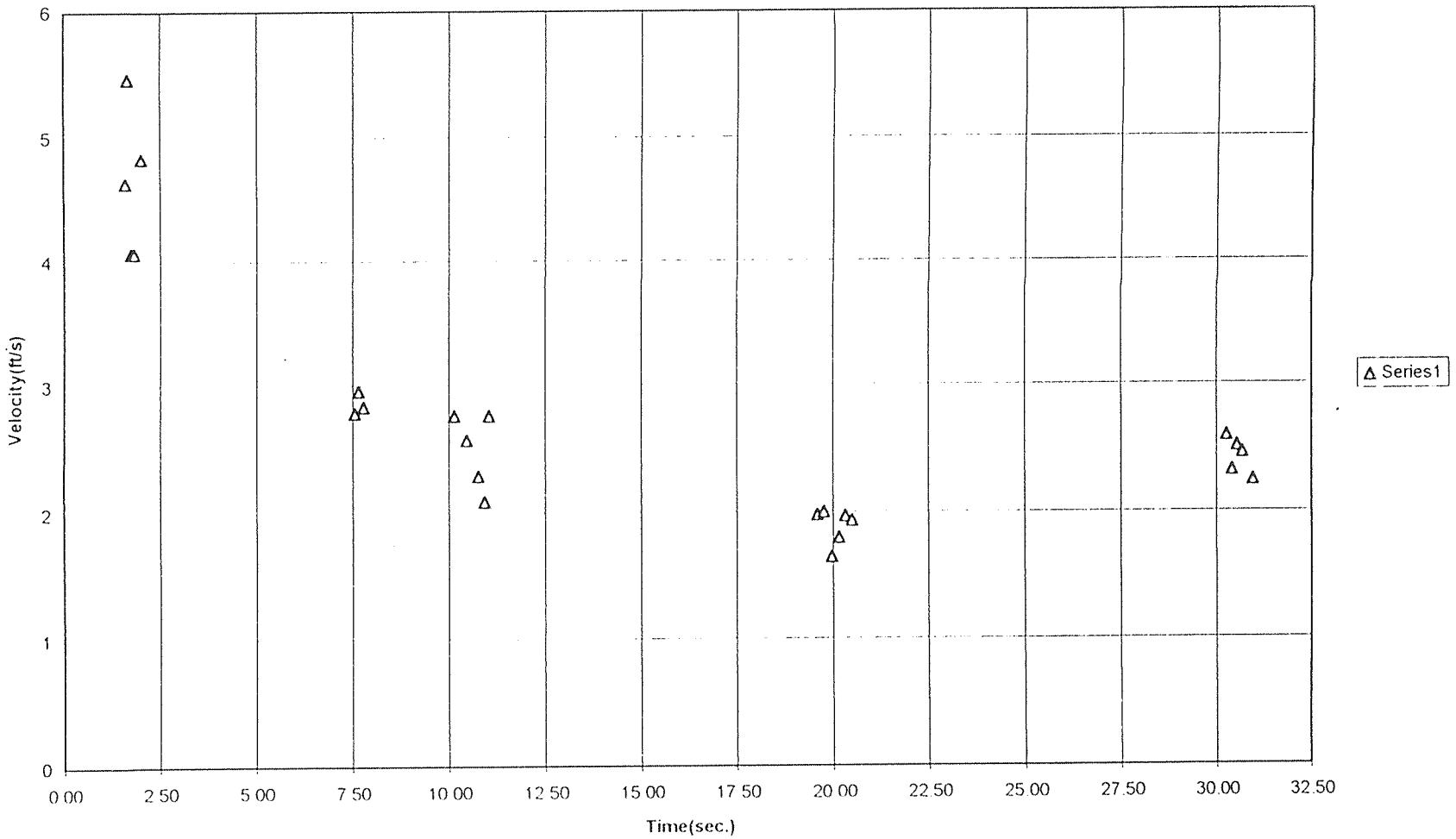

REFERENCES

Dave, R. N., Ashok, A. S., and Bukiet, B. G. (1992). On Development of a Three Dimensional Particle Motion Tracking System. *Proceedings of the ASME Winter Annual Meeting*. Nov. 8-13, 1992, Anaheim, CA.

Dave, R. N., and Bruce, G. B(1995). Non-Intrusive Rigid Body Tracking Technique for Dry Particulate Flows, Part 1: Theoretical Aspects. Submitted to *Review of Scientific Instruments*.

Gupta, V. (1995). Non-Intrusive Tracking System. *Proceedings of the FIFTH ASME Region II Graduate Student Technical Conference*, April 21, 1995, Rutgers University, New Brunswick, New Jersey.

Hanes, D. M. (1991). Experimental Apparatus for the Study of Flowing Granular Materials. *Third Annual DOE/NSF "Flow of Particulates and Fluid" Workshop*, pp. 1-3.

Hanes, D. M. (1992). Observations of Granular Flow in an Inclined Chute. U. S. Department of Energy Flow Advanced Research Objective(GFARO) Report.

Woodcock, C. R., and Mason, J. S., (1987). *Bulk Solids Handling*. Leonard Hill, New York. pp. 47-49.

Ren, S.(1995). Private Communications. New Jersey Institute of Technology, Newark, New Jersey.

Savage, S. B.(1984). The Mechanics of Rapid Granular Flows. *Advances in Applied Mechanics*. Academic Press, Vol. 24, pp. 289-366.

Savage, S. B.(1989). Flow of Granular Materials. *Theoretical and Applied Mechanics*. Elsevier Science Publishers B.V., Amsterdam, pp. 241-246.

Savage, S. B.(1992). Flow of Granular Materials with Applications to Geophysical Problems. A Course of 6 Lectures for Continuum Mechanics in the Environmental Sciences and Geophysics.

Volcy, J. R.(1994). Development of a Non-Intrusive Particle Motion Tracking Technique for Granular Flow Experiments. M. S. Thesis. Mechanical Engineering Department, New Jersey Institute of Technology, Newark, New Jersey.